The $^{3}He(d,p)He^{4}$ Nuclear Fusion Reaction as a Source of Mega-voltage Protons for the Production of Fluorine-18 for PET Applications.

By
Michael Paul Barnes
BSc (Pro) (Hons)

Supervisors: Professor John O'Connor

Assoc/Prof Martin Ebert

A Thesis submitted in the fulfillment of the degree of

Master of Philosophy (Physics)

The University of Newcastle

August 2009

Declaration

I hereby declare that this work contains no material which has been accepted for the award of any other degree or diploma in any university or other tertiary institution and, to the best of my knowledge and belief, contains no material previously published or written by another person, except where due reference has been made in the text. I give consent to this copy of my thesis, when deposited in the university library, being made available for loan and photocopying subject to the provisions of the Copyright Act 1968.

…….

Michael Paul Barnes

October 2008

Acknowledgments

I would like to take this opportunity to thank my two co-supervisors Professor John O'Connor and Associate Professor Martin Ebert for their wisdom, guidance and patience during this project. Their doors and email inbox's were always open to me when I required assistance, feedback or a reality check about my research. I feel I am a better researcher for their help.

Table of Contents

1. Abstract

Fluoro-deoxyglucose (FDG) labeled with fluorine-18 is commonly used in positron emission tomography (PET) imaging. PET imaging is a powerful tool used primarily in the diagnosis and management of cancer. The growth of PET has been limited partly by the difficulties associated in producing fluorine-18. This project involves a theoretical investigation of a novel method of producing fluorine-18 utilising proton generation via the $^{3}He(d,p)^{4}He$ nuclear reaction.

Currently the most common method of producing fluorine-18 for PET is with a medical cyclotron that accelerates protons to mega-voltage energies. These protons are then directed onto a target rich in oxygen-18. This initiates the $^{18}O(p,n)^{18}F$ reaction to produce fluorine-18. The $^{3}He(d,p)^{4}He$ reaction, utilized for the present study, has a Q-value of 18.35 MeV and this results in protons being produced at energies similar to that produced in a medical cyclotron. This reaction was investigated as an alternative proton source for the $^{18}O(p,n)^{18}F$ reaction. The expected advantage of this method over the cyclotron is that particles need only be accelerated to keV energies rather than the tens of MeV that a medical cyclotron accelerates protons to. This is expected to significantly reduce the cost and associated size of the system.

Two systems based on the $^{3}He(d,p)^{4}He$ reaction were designed and calculations were performed to determine the respective yields of fluorine-18. The first system involved separate targets for the $^{3}He(d,p)^{4}He$ and $^{18}O(p,n)^{18}F$ reactions. Helium-3 ions are initially fired onto a deuterated plastic target. A heavy-water (H_2O^{18}) target is placed immediately behind this plastic target to absorb mega-voltage protons produced by the reaction $^{3}He(d,p)^{4}He$ in the plastic. The second system involved a single, super heavy water (D_2O^{18}) target onto which helium-3 is fired so that both the $^{3}He(d,p)^{4}He$ and $^{18}O(p,n)^{18}F$ reactions can occur concurrently in the one target.

The input parameters of energy and beam current for the helium-3 beam required for the $^{3}He(d,p)^{4}He$ reaction were selected on the basis of the performance

of currently available ion sources and in particular the saddle-field ion source. Practical considerations such as radiation safety, target degradation and lifetime and ultra high vacuum (UHV) issues were also investigated to further determine the feasibility of the two systems.

With the beam current and energy at the extreme limits of the saddle-field ion source it was calculated that insufficient fluorine-18 could be produced daily to supply a PET facility with FDG. It was also found that the high helium-3 beam currents and energy required to produce significant amounts of fluorine-18 resulted in prohibitive temperature rises in the targets that would likely result in target vaporization.

2. Aims and Motivation

Positron Emission Tomography (PET) is a nuclear medicine imaging modality with great potential for applications in Oncology and other medical fields. However, the major inhibitor to the widespread use of PET clinically has always been its higher associated costs compared with other nuclear medicine imaging procedures (Ruhlman et al, 1999). These increased costs originate from the expensive equipment and tracer pharmaceuticals associated with PET as well as the common requirement for additional infrastructure for PET procedures (Ruhlman et al, 1999).

Currently, the most common method of producing the widely used PET pharmaceutical, Fluorodeoxyglucose (FDG) is with a medical cyclotron. Such cyclotrons have high initial and ongoing costs, require major infrastructure, are highly resource intensive and require highly skilled personnel to operate. Because of these limitations the growth of PET has been retarded and PET facilities have generally been congregated around centrally located cyclotrons that provide radioisotopes for a number of PET facilities. In general such congregations have centred on major cities and this has provided major logistical problems for rural centres with patients requiring PET scans.

It is the aim of this project to investigate the technical feasibility of an alternative method of producing FDG centred on the $^{3}He(d,p)^{4}He$ nuclear reaction and using a 1 MeV helium-3 beam. This would negate the need for a centrally located cyclotron. Practical issues are superficially discussed to put the technical feasibility into context, but it is not the aim of this project to perform a full feasibility study. It is anticipated that a system could be developed that can be installed and operated in any PET facility as and when FDG is required. This would greatly assist the growth of PET particularly into regional and isolated areas.

Conceptually, two different systems based on the $^{3}He(d,p)^{4}He$ reaction are investigated using theoretical calculations of FDG yield. Practical considerations for these systems are also briefly investigated.

3. Introduction

3.1 Positron Emission Tomography (PET) and its Applications

Positron Emission Tomography (PET) is a powerful metabolic imaging technique that has been shown to impact significantly on the treatment of patients (Bailey et al, 2004). PET is primarily utilised in oncology but is also used in cardiology and neurology. To perform a PET scan a radiopharmaceutical containing a positron emitting isotope is injected into the patient. The most commonly used radiopharmaceutical is Fluorodeoxyglucose (FDG), which utilises fluorine-18 as the positron emitter. After a period of time to allow the FDG to be transported around the body and metabolised, the PET scan is performed by placing the patient at the centre of a ring of coincidental X-ray detectors, usually scintillation detectors.

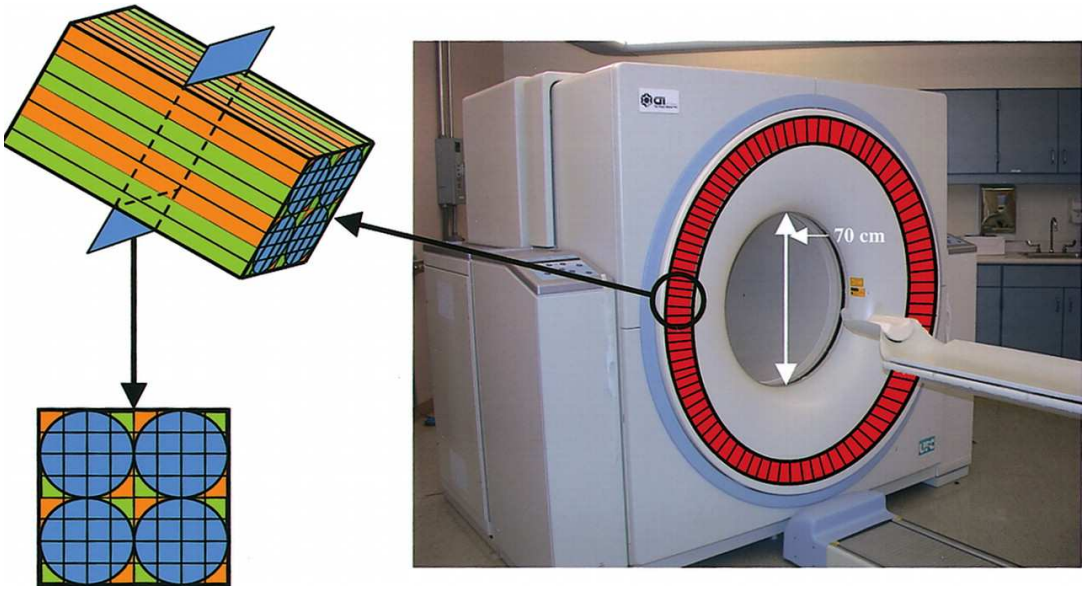

Fig 1 Photograph (frontal view) of a hybrid PET-CT scanner showing the PET ring detector system (red ring). There are up to 250 block detectors in the ring. Drawing shows a detector block with 8 x 8 smaller scintillation crystals (green and orange rectangles) linked to four photomultiplier tubes (blue circles). The PET ring is in the PET gantry at the back, but is shown for ease of illustration at the front. Adapted from Kapoor et al, 2004.

FDG is a glucose analogue and is absorbed and metabolised in the body the same as glucose. It is the imaging of the metabolic process that is clinically useful. Because of the decay of fluorine-18 in the FDG molecule, positrons are produced at the sites of FDG uptake. These positrons can move a short distance (~1-3 mm) before coming to rest and into contact with an electron where the particles annihilate and two photons, each of energy 511 keV, are produced. This energy is equivalent to the electron/positron rest mass and as a consequence of the conservation of momentum, the photons depart in opposite directions. Once these photons leave the patient the ring of detectors can detect them. If a pair of detectors both register a photon within a small time interval known as the 'coincidence time window' (Sprawls, 1993) the straight line between the two detectors, known, as the 'line of response' (LOR) (Sprawls, 1993), can be stored digitally. A large number of acquired LOR's can be used to reconstruct an internal image of the distribution of FDG in the patient. Image intensity will provide a map of FDG metabolism in the patient, which can provide unique diagnostic information.

3.1.1 Clinical Applications of PET

At present PET is used clinically for three main areas of diagnosis and management:

- Cancer diagnosis and management
- Cardiology and cardiac surgery
- Neurology and psychiatry.

(Bailey et al, 2004).

PET has revolutionised the management and diagnosis of many types of cancer. It has been shown that PET has altered patient management significantly in more than 25 % of patients of all cancer patients and up to 40 % for some specific diseases (Bailey et al, 2004). Specifically, PET has been found to have use in the diagnosis of malignancy, such as in differentiating malignant from benign pulmonary nodules. PET is also beneficial for grading a known malignancy as FDG

uptake correlates with the degree a tumour is malignant. One of the most important facets of PET in oncology is in staging the disease to determine how wide spread the disease is in the patient. PET can also be used following treatment to determine how much, if any, of a tumour is still viable (Bailey et al, 2004).

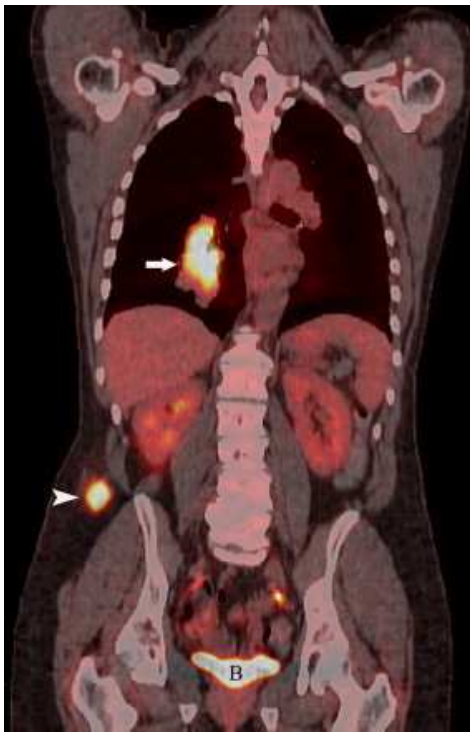

Fig 2 An example of an FDG PET scan used in Oncology. Image shows increased uptake of FDG within the primary malignancy (*arrow*). There is increased FDG uptake in a soft-tissue mass (*arrowhead*). B, accumulation of FDG in the bladder. Biopsy results confirmed small-cell lung cancer. Adapted from Erasmus and Sabloff, 2008

In cardiology two things are currently tested using PET. Firstly, Rubidium-82 PET can be used to measure myocardial perfusion to assess the functional significance of coronary artery disease. This test essentially measures blood flow and is expected to increase in demand in the near future (Bailey et al, 2004). The second test that PET can be used for in the field of cardiology utilises FDG PET to assess the viability of a jeopardised myocardium. This is important because the risks and benefits of medical treatment in advanced coronary artery disease are dependent on the condition of viable but hibernating myocardium (Bailey et al, 2004).

Evolving fields in which PET is proving successful are in the fields of Neurology and psychiatry. Its applications in this field include management of brain tumours and the pre-surgical work-up of patients with epilepsy resistant to standard medical therapies. PET has also been shown to exceed all other methods for diagnosis and differential diagnosis of dementia (Bailey et al, 2004).

3.1.1.1 Positron Decay

Positron decay is the form of beta decay that occurs in proton-rich nuclei. In positron decay the nucleus achieves greater stability by converting a proton into a neutron in the nucleus by nuclear transmutation. The general equation for positron decay is:

$$ {}^{A}_{Z}X \rightarrow {}^{A}_{Z-1}Y + {}^{0}_{1}\beta^{+} + \upsilon + Q \qquad (1) $$

Where: X = parent nucleus
Y = daughter nucleus
β^{+} = positron
υ = neutrino
Q = energy
A = Atomic mass number
Z = Atomic number

The daughter nucleus has an atomic number one less than the parent so the daughter must eject an orbital electron to balance the charge within the atom. This is often achieved via the process of internal conversion where the nucleus supplies enough energy to an orbital electron to overcome the binding energy and exit the atom. In this scenario both a positron and an electron have been emitted from the atom so the daughter nucleus must be at least two electron masses lighter than the parent nucleus.

3.1.1.2 Annihilation

Once Positron decay has occurred the positron traverses the surrounding matter, undergoing the same type of interactions as an electron does. This includes ionisation, excitation and bremsstrahlung processes. As the positron loses energy,

the annihilation cross-section increases and eventually the positron will combine with a nearby electron. For a short time a likely event is that a metastable species called positronium is formed where the positron and electron revolve around their combined centre of mass. Positronium is a non-nuclear, hydrogen-like element that has a mean lifetime of around 10^{-7} seconds, after which the positron and electron annihilate.

During the annihilation process the combined electron and positron mass is converted into energy according to Einstein's equation,

$$E = mc^2 \qquad (2)$$

Where: E = Energy
m = relativistic mass
c = the speed of light in vacuum

As the positron and electron are essentially at rest subsequent to annihilation they each have a total energy equal to the rest energy of approximately 511 keV. This yields 1022 keV energy from a single electron/positron annihilation event and this energy usually manifests as two photons of 511 keV. In less than 1 % of cases three photons are produced at about 340 keV (Bailey et al, 2004). In the two photon case the conservation of momentum requires that the photons travel in opposed directions. An example of positron decay followed by positron/electron annihilation is shown in figure 3 for the decay of fluorine-18.

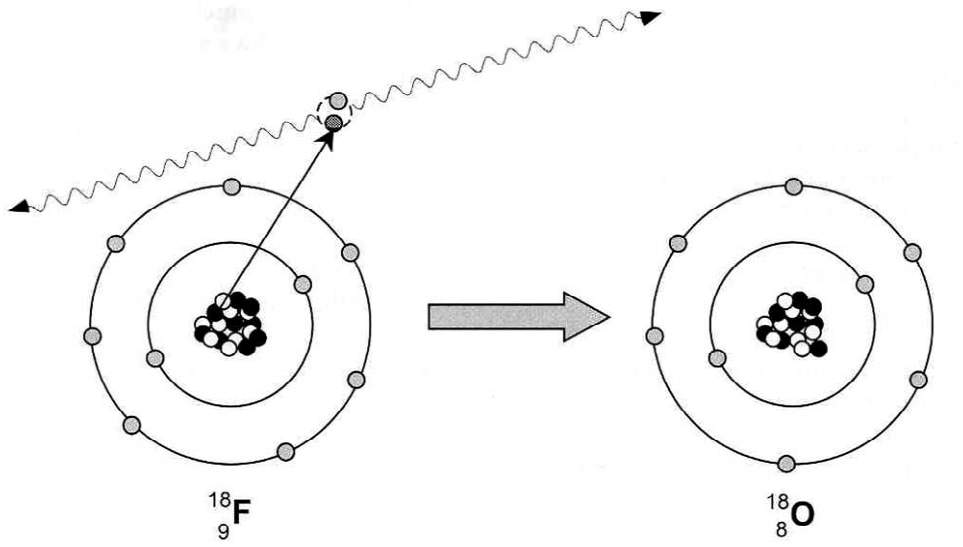

Fig 3 Positron decay of fluorine-18 to oxygen-18 with subsequent positron/electron annihilation. Adapted from Bailey et al, 2004.

The nature of the positron decay and the annihilation event are both important for producing good PET images. The greater the positron energy following positron decay, the greater the range it will have before slowing enough to annihilate with an electron. It is the point at which the positron is produced that ideally is of interest in PET. However, it is the point of annihilation that is detected via the product photons. Therefore, the greater the positron range the less valid is the approximation that the point of positron emission and the point of annihilation are essentially the same. This results in a decrease in image resolution as positron energy increases. Another mechanism in which positron energy affects resolution involves the concept that the annihilation photons are emitted exactly opposite one another. This concept only holds true if the positron and electron have zero velocity at the time of annihilation. If there is some velocity then the annihilation photons will have a component of momentum parallel to this velocity. Hence, the Line Of Response (LOR), which is the line connecting two coincident detectors, for this event will not intersect the point at which the annihilation reaction occurred causing blurring of the image.

3.1.2 Positron Emitters

The properties of the positron emitting isotope are often the source of limitation for PET images. The half-life of the isotope has implications for producing fluorine-18 when the physical distance between production facilities and the patient is large as well as for subsequent disposal of waste from the imaging process. Radiation safety in manual handling of the isotope depends on half-life and the quality of emitted radiation. The emitted positron energy influences image quality due to the reasoning outlined in the previous section. Isotope half-life also influences image quality because a short half-life results in increased activity and hence more counts are registered by the detectors resulting in better statistics.

The chemical properties of the positron emitter are also important. The isotope must be able to be tagged to a molecule that is preferentially taken up in some organ of the body and so able to indicate a medical condition. The positron emitter must also be non-toxic to the patient and not decay to a toxic species. Another important feature of a positron emitter for its suitability for PET is that it can be produced relatively cheaply and easily and its synthesis to a radiopharmaceutical must also be relatively straight forward and inexpensive.

3.1.2.1 Fluorine-18

Fluorine-18 tagged to FDG is the most commonly used PET radionuclide (Bailey et al, 2004). Usually fluorine-18 is produced in a Medical cyclotron. Its half-life of 110 minutes is well suited for PET in that it provides high enough activity to produce acceptable count statistics in PET scanning and is long enough to allow transport of up to about 200 km from the cyclotron to the PET scanner (Ruhlman et al, 1999). fluorine-18 decays primarily by positron emission (97%) and by only a proportionately small amount by Electron Capture (3%) (Bailey et al, 2004). Upon decay of fluorine-18 positrons have a maximum kinetic energy of 0.635 MeV resulting in a maximum linear range in tissue of 2.4 mm, which allows for a resolution limit of approximately 5 mm (Ruhlman et al, 1999). Fluorine is biologically inert and fluorine-18 decays to oxygen-18, which is also biologically

inert. Fluorine can be substituted for hydrogen in many compounds (Sprawls, 1995) and its synthesis into FDG has become common practice.

3.1.2.2 Other Positron Emitters

Carbon-11, oxygen-15 and nitrogen-13 are the next most commonly used PET isotopes after fluorine-18 (Bailey et al, 2004). Extensive research has also been made for using other positron emitters such as radiohalogens like bromine-76, iodine-122 and iodine-124 and with a number of metals including copper, gallium and rubidium isotopes. Physical properties for some common PET isotopes are presented below (table 1).

Table 1 Physical properties of a selection of common positron emitters used for PET (Bailey et al, 2004).

Isotope	**Half-life**	**Decay Modes (%)**	**Max β^+ Energy (MeV)**
fluorine-18	109.8 min	β^+(97) EC(3)	0.635
carbon-11	20.4 min	β^+(100)	0.96
oxygen-15	2.1 min	β^+(100)	1.72
nitrogen-13	9.9 min	β^+(100)	1.19
bromine-76	16.1 hours	β^+(57) EC(43)	3.98
iodine-122	3.6 min	β^+(77) EC(23)	3.12
rubidium-82	1.25 min	β^+(96) EC(4)	3.15

3.1.3 Fluorodeoxyglucose (FDG)

Fluorodexoyglucose, FDG (2-[^{18}F]fluoro-2-deoxy-D-glucose) is the most used and most studied PET radiopharmaceutical. FDG is a glucose analogue and hence, its uptake and metabolism in the body is similar to that of normal glucose. FDG PET was originally used for diagnosing changes in the heart or brain but is now used principally for oncology (Ruhlman et al, 1999).

3.1.3.1 FDG Synthesis

The production procedures of FDG differ slightly from manufacturer to manufacturer and only limited information is available about these procedures (Ruhlman et al, 1999). Biochemically, FDG is a non-physiological analogue of glucose and the fluorine-18 labeling is initially accomplished by nucleophilic substitution on 1,3,4,6-tetra-O-acetyl-2-trifluoromethanesulfonyl-manno-pyranose. (Ruhlman et al, 1999). From this, the acetyl groups are removed by a process of hydrolysis in hydrochloric acid before the product is purified chromatographically in the presence of ion-retardation resin. At this stage the product is acidic with a pH of about 4. The solution is made neutral by the addition of a specific amount of buffered Sodium Chloride before the solution undergoes sterile filtration to yield 2-[^{18}F] FDG with a pH of 7 that can be used for PET (Ruhlman et al, 1999).

Once synthesised FDG is a sterile, colourless to light yellow, non-combustible liquid. A typical batch has a volume of about 14.5 ml and a specific activity ranging between 1 and 10 GBq/μmol (Ruhlman et al. 1999).

Fig 4 The TRACERlab FX_{F-E} system for the synthesis of general fluorine-18 tracers via electrophilic substitution with [^{18}F] fluorine in the form of F_2.

FDG synthesis does not approach 100 % efficiency. Two modern systems have been shown to have efficiencies of 69 % and 53 % respectively (Yuan-Hao Liu et al, 2006). Quality Control (QC) testing is mandatory post synthesis, resulting in a further reduction in fluorine-18 activity. Typically, QC testing takes about 30 minutes and thus the amount of activity available for injection is about 40 to 50 % of

the starting activity. For the purposes of this study the upper limit of 50 % loss of activity between fluorine-18 production and injection will be used.

3.1.3.2 FDG Dosage

The dosage of FDG required for a single patient scan is dependent on the type of scanner being used, the target organ being scanned and the required image quality (Ruhlman et al, 1999). FDG dose is prescribed in terms of activity and for a single scan the administered activity can range from 185 to 740 MBq, although the majority of centres use dosages ranging from 185 to 370 MBq (Ruhlman et al, 1999). Children receive smaller dosages of 96 MBq or less. These dosages allow for decay between the time of administration and the time of scan. This time period is usually 30 to 60 minutes after injection to allow the FDG to be transported around the body and the metabolic process to begin. It has been estimated that administered activity will increase in the future in the quest for improved image quality. A recent study by Everaert et al, (2003) recommended that 8 MBq per kilogram of patient body weight was required to produce high quality images.

3.2 The $^{18}O(p,n)^{18}F$ Reaction

The $^{18}O(p,n)^{18}F$ reaction is the most common reaction used to produce fluorine-18. This is because of the relative ease with which oxygen-18 can be obtained. Oxygen-18 has a natural abundance of about 0.2 % (Krane, 1988) and can easily be produced commercially by the fractional distillation of natural water (Fawdry, 2004). The technique is based upon the isotope effect where there is a small preference to remove the lighter isotope in the distillate leaving the heavier isotopes to concentrate in the residue. After multiple distillations the composition of the residue tends towards D_2O^{18} with more than 95 % enrichment (Fawdry, 2004). This so called 'super heavy water' is ideal for use in this project (see section 4.4.2), but $^{18}O_2$ gas can be produced from D_2O^{18} by electrolysis and later combined with Hydrogen gas to form H_2O_{18}.

The Q-value for the $^{18}O(p,n)^{18}F$ reaction is approximately –2.4 MeV (Nickles et al, 1986). And protons of such energy can easily be produced in cyclotrons, Van De Graaff generators and high-energy linear accelerators. This

relatively small Q-value is another reason why the $^{18}O(p,n)^{18}F$ reaction is most commonly used for fluorine-18 production.

Extensive work has been performed to determine the $^{18}O(p,n)^{18}F$ reaction cross sections for various incident proton energies (Kitwanga et al, 1990, Blair and Leigh, 1960, Bair, 1973.). The results of this work are presented in the paper by Takacs et al (2003). From Takacs' compilation of $^{18}O(p,n)^{18}F$ cross section data, selected data was modeled with a Pade fit which is a version of spline fitting (Takacs et al, 2003). Major resonances in the data are accounted for in the fit but an associated error between 15 and 30 % is observed. Takacs' fit provides an update to the recommended cross section data published by the IAEA in 2001 as new data has been included in the fit (Takacs et al, 2003). The recommended cross section data of Takacs for the $^{18}O(p,n)^{18}F$ reaction is presented (figure5).

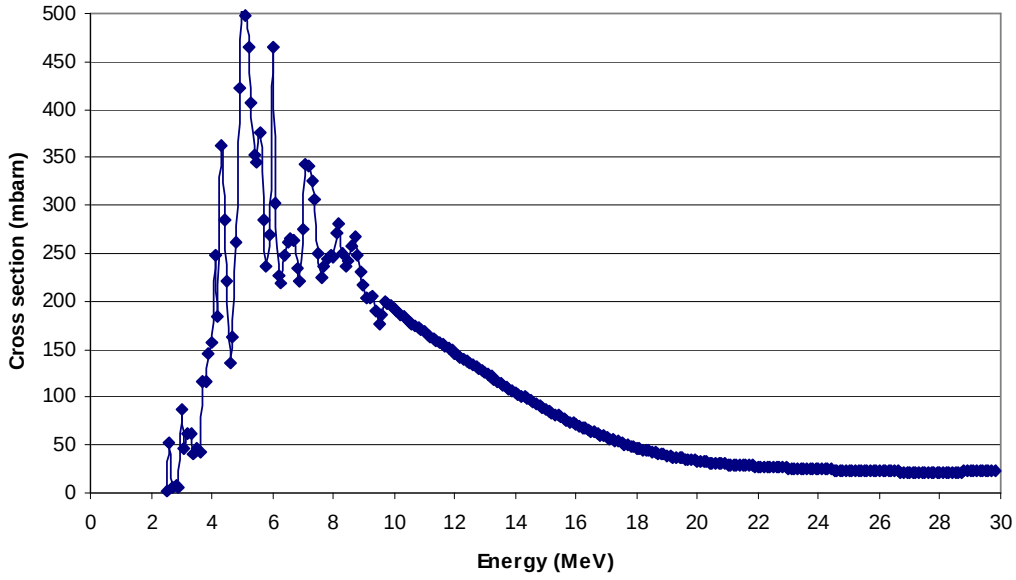

Fig 5 Recommended Cross sections for the $^{18}O(p,n)^{18}F$ reaction. Takacs et al, 2003.

Figure 5 shows that in the incident proton energy range of 0 to 30 MeV the cross section for the $^{18}O(p,n)^{18}F$ reaction is maximum at about 5 MeV. At this energy the cross section is 498 mbarn though one author claims a cross section of approximately 600 mbarn at this point (Kitwanga et al, 1990). Figure 5 shows that

the cross section is 0 below about 2.5 MeV, resulting from the 2.4 MeV Q-value of the reaction. Between 2.5 MeV and 10 MeV the cross section data appears quite noisy with a number of resonance peaks. Some of the major peaks in cross section are seen at 4.3, 6 and 7.2 MeV where the cross sections are 363, 465 and 342 mbarn respectively. Above 10 MeV the fit is smooth and gradually declines at a decreasing rate. This region has been smoothed due to the small number of data sets available in this region and the inconsistency between the data that is available (Takacs et al, 2003).

3.3 Cyclotron Production of Fluorine-18 Utilizing the $^{18}O(p,n)^{18}F$ Reaction

The most common method of producing nucleophilic fluorine-18 for PET is via the $^{18}O(p,n)^{18}F$ nuclear reaction induced by megavoltage protons accelerated in a cyclotron (Bailey et al, 2004). Although fluorine-18 is the predominant radioisotope used in PET an advantage of using a cyclotron is that other useful PET isotopes such as carbon-11, nitrogen-13 and oxygen-15 can also be produced with the same system.

Fig 6 The CTI RDS111 Medical single particle cyclotron commonly used for the production of fluorine-18.

Cyclotrons used for PET isotope production generally come in two main forms, either single particle cyclotrons that are capable of accelerating protons to about 10-11 MeV or dual particle 18 MeV cyclotrons that can accelerate either protons or deuterons. It is the single particle cyclotrons that are most commonly used, as they are cheaper to buy initially. However, dual particle cyclotrons have the advantage of being able to produce Bromine-76, Iodine-124 and Copper-64 positron emitting isotopes in addition to the four common isotopes already mentioned.

A cyclotron operates by accelerating charged particles in electromagnetic fields. At the centre of the cyclotron an ion source produces negatively charged ions. These ions are singly ionised hydrogen in proton accelerators. A magnetic field is applied and causes the hydrogen ions to travel in a circular path around the cyclotron. Two powerful Dee shaped electrodes are situated on either side of the ion source. Electric fields between the dees accelerate the particles with each lap around the cyclotron. The polarity of these electric fields are reversed at the cyclotron frequency so that the particles are accelerated every time they come to the gap between the dee's (twice per lap). The acceleration of the particles causes their path to become a spiral of ever increasing radius obeying the Lorentz force law until the particle energy becomes large enough so that they collide with a stripping foil.

$$F = q(E + v \times B) \qquad (3)$$

where: F = force
q = the particles charge
E = Electric field strength
v = particles velocity
B = magnetic field strength

At the stripping foil the hydrogen ion's (H^-) electrons are stripped away leaving a positively charged proton. Because of this change in charge from negative to positive, the curvature of the proton's orbit in the magnetic field reverses. The proton is thus targeted onto a H_2O^{18} target for fluorine-18 production. The protons, whose energy is now in the order of 10 to 20 MeV can interact with the oxygen-18

to initiate the $^{18}O(p,n)^{18}F$ reaction and hence produce fluorine-18 (Sprawls, 1995). Single-particle cyclotrons can typically produce approximately 111 GBq of fluorine-18 in an hour of beam on time, which can be synthesised into approximately 37 GBq of FDG. This is sufficient for 10 to 20 patient PET scans (Ruhlman et al, 1999).

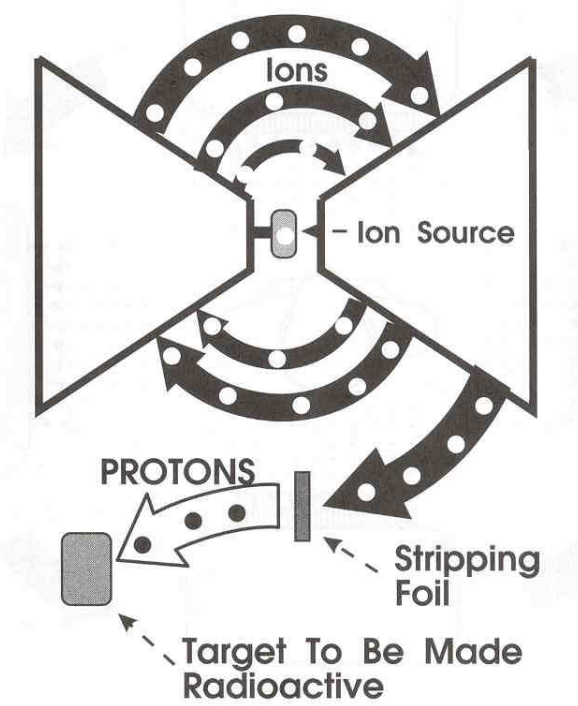

Fig 7 Schematic diagram of a Medical Cyclotron. Adapted from Sprawls, 1995.

3.4 Alternate Production Methods of Fluorine-18

3.4.1 Alternate Methods using the $^{18}O(p,n)^{18}F$ reaction

3.4.1.1 Linear Accelerators

Megavoltage protons for initiating the $^{18}O(p,n)^{18}F$ reaction to produce fluorine-18 for FDG synthesis have been accelerated using high energy linear accelerators. One such linear accelerator is the PULSAR system developed by Accys Technology Inc. The PULSAR system targets 7 MeV protons at about 100 μA onto an oxygen –18 water target (Robinson and Hamm, 1997). For a 1 hour irradiation with a beam of these specifications 55.5 GBq of fluorine-18 is produced.

3.4.1.2 Lasers

Promising research and development is currently ongoing towards using a laser system to produce fluorine-18. This research shows much promise but has yet to produce a system that has been used clinically. It has been shown that laser/plasma interactions can accelerate protons to energies up to about 58 MeV (Fritzler et al, 2003). When a laser is focused to high intensity onto solid targets a plasma is created. Free electrons within the plasma readily absorb the photons of the laser and are accelerated in the process. The accelerated electrons propagate through the target and set up a space-charge field when they exit (Fritzler et al, 2003). This sets up a strong static-electric field that can accelerate ions perpendicularly to the target surface. Protons from the plasma are hence accelerated with a broad Maxwellian-like spectrum that can be used to initiate the (p,n) reactions such as the $^{18}O(p,n)^{18}F$ reaction to produce fluorine-18 or other positron emitting isotopes suitable for PET (Fritzler et al, 2003).

Most research involving lasers for medical isotope production has utilised large Nd:Glass lasers (Fritzler et al, 2003). Such lasers have a repetition rate of about one shot every 20 minutes and although activities in the order of 100 kBq of medical isotopes have been produced the low repetition rate has limited their practical use (Ledingham et al, 2004). An example of a Nd:Glass laser used for research as a fluorine-18 producer is the petawatt Vulcan laser at the Rutherford Appleton Laboratory. Using this laser Ledingham et al, 2004 produced protons of energy up to 50 MeV with laser peak intensity at $2x10^{20}$ $W.cm^{-2}$. These protons were then targeted onto a H_2O^{18} target from which 100 kBq of fluorine-18 were produced via the $^{18}O(p,n)^{18}F$ reaction (Ledingham et al, 2004).

At present the research revolves around smaller “table-top” sized lasers such as Ti:sapphire lasers that have repetition rates in the order of 10 Hz. If such a laser could be used to produce clinically adequate amounts of isotope then it would have a number of advantages over current techniques. Firstly, the accelerating fields can exceed GV/m, cutting down the accelerating length to tens of microns. Secondly, such laser systems are quite compact and cheap and thirdly, no shielding for radiation protection is needed up to the point where protons are produced (Fritzler et

al, 2003). Using such a Ti:sapphire laser operated at 6 x 10^{19} W.cm^{-2} at repetition rate of 10 Hz for 30 minutes, Fritzler et al managed to produce 13 MBq of carbon-11 and this can be extended to GBq using similar lasers with kilohertz repetition rates. Similar results were found with fluorine-18 production (Fritzler et al, 2003).

3.4.2 Methods using alternate reactions

3.4.2.1 Cyclotrons

The $^{18}O(p,n)^{18}F$ reaction is not the only reaction from which cyclotrons have been used to produce fluorine-18. Other reactions used have included the $^{20}Ne(d,\alpha)^{18}F$ and the $^{16}O(^{3}He,p)^{18}F$ reactions.

3.4.2.1.1 $^{20}Ne(d,\alpha)^{18}F$

The method of producing fluorine-18 via the $^{20}Ne(d,\alpha)^{18}F$ reaction is well established (Guillaume et al, 1991). Several independent centres (Casella et al, 1980, Blessing et al, 1986, Guillaume et al, 1991) have routinely produced Carrier-Added fluorine-18 with this reaction. The method these centres use is ostensibly the same with some small variations in some of the physical parameters. The method involves bombarding high pressure Neon gas (up to 25 bar) with moderate energy deuterons (11 to 14 MeV) accelerated in a cyclotron. The neon gas used for the target is required to be 99.998 % pure and in particular needs to be free of carbon oxides, nitrogen and fluorocarbons which can drastically affect the chemical form of the recovered fluorine-18 (Guillaume et al, 1991). The target body is preferably made of nickel and a small amount of fluorine (~2 %) is added to the Neon prior to irradiation. These two factors aid the fluorine-18 recovery process. In the absence of added fluorine, fluorine-18 diffuses to the target wall and is chemically absorbed as nickel fluoride. When carrier fluorine is present, exchange of nucleogenic fluorine-18 competes with surface absorption and recovery of fluorine-18 becomes possible (Guillaume et al, 1991). fluorine-18 yields of up to 91.9 mCi/μA have been reported (Casella et al, 1980) but difficulties with nickel targetry and gas handling systems for the neon/fluorine target are problematical for routine use (Guillaume et al, 1991).

3.4.2.1.2 $^{16}O(^{3}He,p)^{18}F$

The $^{16}O(^{3}He,p)^{18}F$ reaction has been researched for use in producing fluorine-18 for PET imaging (Tilbury et al, 1970, Bishop et al, 1996). Thick target yields from this reaction are low compared with the $^{20}Ne(d,\alpha)^{18}F$ and $^{18}O(p,n)^{18}F$ reactions but it has the great advantage of using an inexpensive target material ($[^{16}O]H_2O$) (Bishop et al, 1996). Megavoltage helium-3 irradiation of water primarily yields fluorine-18, but a large number of other products are produced with half-life of 2.1 minutes and less (Tilbury et al, 1970). In the work of Bishop et al (1996), it was found that irradiation of oxygen-16 water with a 26.8 MeV helium-3 beam could produce a saturation yield of up to 34 mCi/μA for an electroformed Nickel target. Such a target allows for 89 % recovery of the product fluorine-18 and it has been estimated that a typical production type irradiation could produce enough FDG for two patient PET examinations (Bishop et al, 1996). For practical feasibility a higher yield is required. This can be achieved by increasing the helium-3 energy to about 40 MeV, however such energies require powerful accelerators that are not common and are expensive to operate. For this reason the $^{16}O(^{3}He,p)^{18}F$ reaction is not routinely used for fluorine-18 production (Guillaume et al, 1991).

3.4.2.2 Nuclear Reactors and Van de Graaff Generators

Nuclear reactors have been extensively studied for the production of fluorine-18 (Guillaume et al, 1991). It has been found that reactors capable of a thermal neutron flux of 1.0×10^{13} $cm^{-2}s^{-1}$ can produce sufficient fluorine-18 (1 to 4 MBq) to produce quantities of FDG useful for PET (Guillaume et al, 1991). The procedure to produce fluorine-18 in a reactor is a two step process. First, the thermal neutrons produced in the reactor are incident on a Lithium target. The Lithium target is usually in the form of Li_2CO_3 but $LiOH{\cdot}H_2O$ or $LiNO_3$ have also been used (Ramirez et al, 1992). The Lithium target is enriched in Lithium-6 (Tilbury et al, 1970) and is either in the dry state or is moistened with doubly distilled water. When thermal neutrons impinge on the lithium target the $^{6}Li(n,\alpha)t$ reaction occurs. The tritons produced in this reaction are then free to travel through the target, possibly coming into contact with oxygen-16 atoms where the

$^{16}O(^{3}H,n)^{18}F$ reaction can take place producing fluorine-18. The target must be chemically treated to acquire the fluorine-18 and this process produces significant practical difficulties, primarily due to the need to isolate the product from tritium and Lithium (Guillaume et al, 1991).

Another method of producing fluorine-18 using the $^{16}O(^{3}H,n)^{18}F$ reaction involves accelerating the tritons to 3 MeV directly using a Van de Graaff generator (Tilbury et al, 1970). This method is advantageous in that while tritium must still be removed from the product, the lithium target is not required making the chemical separation of fluorine-18 less complicated. Difficulties in acquiring and storing tritium and the associated radiation protection issue have limited this method of fluorine-18 production.

3.5 The $^{3}He(d,p)^{4}He$ Reaction

Helium-3 fusion with Deuterium to produce helium-4 and a proton is a well known reaction due to interest in it as a source of fusion power. One of its most attractive features for fusion power is its Q-value of 18.35 MeV (Geist et al, 1999). As most of this energy goes to the proton due to conservation of momentum considerations (see section 5.3.4) the $^{3}He(d,p)^{4}He$ reaction can be used as a source of megavoltage protons.

Helium-3 is a relatively rare helium isotope with natural abundance of approximately 1.38×10^{-4} % (Krane, 1988). It is naturally produced via tritium decay. Helium-3 is relatively difficult to produce as demonstrated by proposals to mine it on the moon where there are large deposits. However, helium-3 can still be purchased relatively easily from companies such as Icon Isotopes Ltd, Spectra Gases Inc and Chemgas Inc.

The $^{3}He(d,p)^{4}He$ reaction cross sections for various incident particle energies have been the subject of research since the 1950's (Bonner et al, 1952, Moller and Besenbacher, 1980 & Geist et al, 1999). For energetic helium-3 particles onto stationary deuterium atoms over the energy range 0 to 1000 keV, the work of Moller and Besenbacher, (1980) is the most comprehensive. Moller and Besenbacher determined total cross sections from proton yields measured with

surface-barrier detectors. Helium-3 ions were accelerated using a Van der Graaff generator. A mathematical function was fit to the measured data and is presented as equation 4 and figure 8

$$\sigma_{tot} = A\frac{\varepsilon^{B}\left(Ce^{-D\varepsilon} + E\right)}{\varepsilon^{B} + Ce^{-D\varepsilon} + E} \qquad (4)$$

where: σ_{tot} = total cross section in millibarns
ε = Helium-3 laboratory energy in MeV
A, B, C, and E are fit parameters
A = 1.577×10^{4}
B = 3.53
C = 2.921×10^{-1}
D = 2.411
E = 7.93×10^{-3}

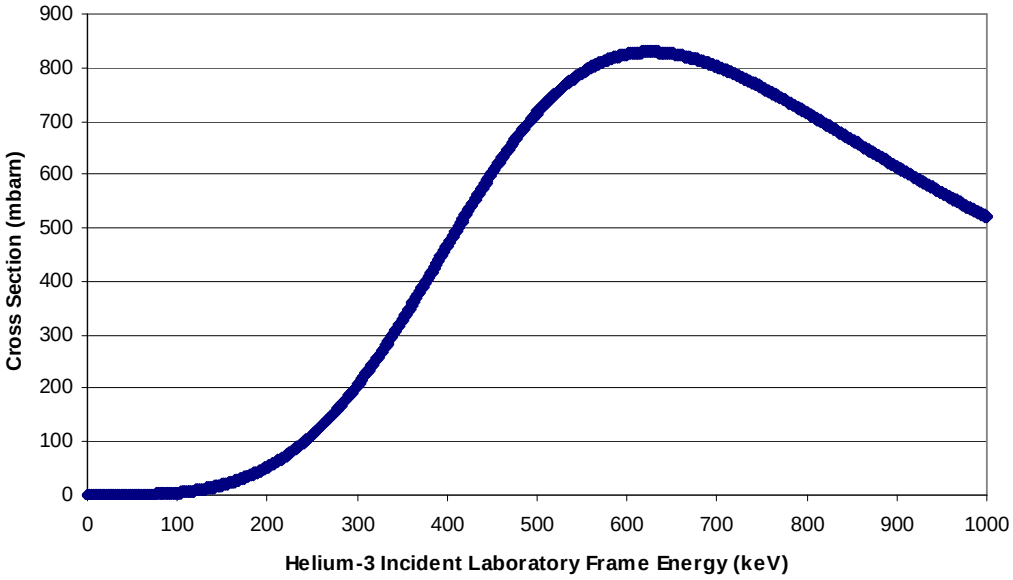

Fig 8 Recommended Cross sections for the $^{3}He(d,p)^{4}He$ nuclear reaction. Moller and Besenbacher, (1980).

The fit describes the cross section with an accuracy of ± 1.5 % at energies up to 1 MeV. Accounting for experimental errors in the data it has been estimated that the fit describes the total cross section for the $^{3}He(d,p)^{4}He$ reaction with an accuracy of ± 4 % up to a centre-of-mass energy of 500 keV and an accuracy of ± 5

% up to 1 MeV (Moller and Besenbacher, 1980). Cross section data reported in previous literature differ typically by approximately 5 % but as much as 30 % at the peak. (Moller and Besenbacher, 1980). Moller and Besenbacher also found the differential cross section to be isotropic to within 1 % in the centre-of-mass system.

3.6 Helium-3 Ion Sources

To produce mega-voltage protons using the $^{3}He(d,p)^{4}He$ reaction the first required process is to accelerate helium-3 nuclei to energies of between about 300 and 1000 keV. At these energies the $^{3}He(d,p)^{4}He$ reaction cross section is maximised (Geist et al, 1999). Work has been undertaken in both industry and research to produce ion beam sources of varying characteristics to fulfill a number of applications including those associated with ion beam milling, ion beam etching and sputtering.

To initiate the $^{3}He(d,p)^{4}He$ reaction an ion source is required with fairly specific characteristics. The source must be capable of first ionising inert gas atoms and then accelerating the inert gas ions to energies in the order of hundreds of keV. A high beam current of protons is required to produce fluorine-18 and this means that an even higher current of helium-3 is required to compensate for inefficiencies in producing protons via the $^{3}He(d,p)^{4}He$ reaction. The highest current negative ion beam source capable of producing kilovoltage ion energies was a Plasma source developed by Kuroda, 1997. Kuroda's source is capable of producing negative ions at 120 keV at a beam current of 16 A. Such a source is expensive, dangerous and could cause significant thermal damage to a deuterium target, but represents an upper limit in ion beam current for negative ion sources.

As it is hoped to eventually use the device clinically, there are a number of practical considerations that an ion source must meet. As the device is intended to be operated by medical staff without specific knowledge of ion sources then the ion source must be simple and safe to operate, reliable and require minimal maintenance.

3.6.1 Saddle-Field Ion Sources

Based on the ion source requirements the saddle-field ion source seemed a good possible candidate. The Saddle-Field ion source is a magnetic-field-free ion source that operates at low gas pressure without the need for an electron emitting filament (Godechot et al, 1990). The source utilises a cold cathode, has a long lifetime, is reliable and is rugged. It works by inducing free electrons to oscillate between two cathodes under the action of a DC field (Franks, 1984). Free electrons in the vicinity of a cathode travel through the anode region towards the opposite cathode, where their motion is retarded and then accelerated back towards the anode region once more for the process to be repeated with the other cathode. The electrons oscillate about a central saddle point in the potential field with relatively long path lengths before finally being captured by the anode. Because of the long path length, when a gas is allowed to enter into the system the chances of ionisation are high. The ions formed travel radially towards the cathode and emerge along straight paths (Franks, 1984). Saddle-field ion sources are by their nature area sources. However, conversion to a narrow beam is easily attained by collimation, but at considerable loss of beam current. A schematic of a saddle field ion source is given in figure 9.

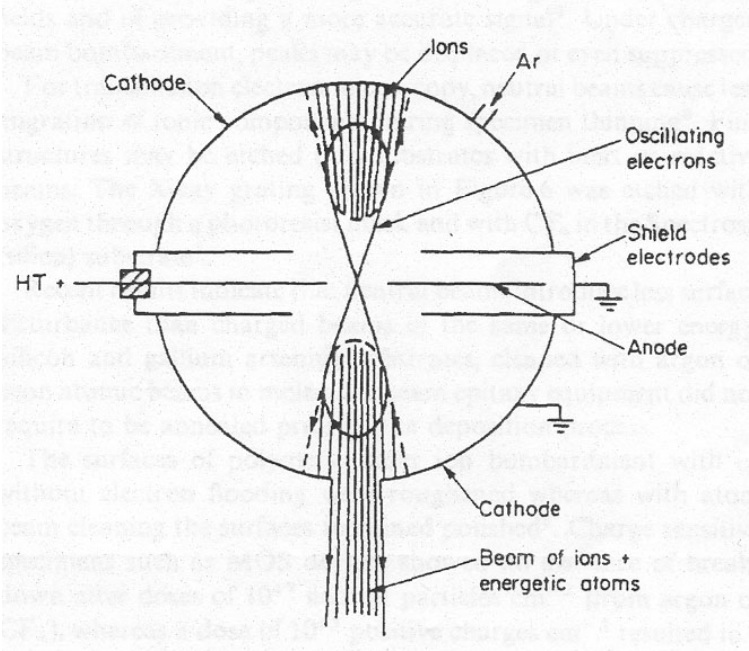

Fig 9 Schematic diagram of a saddle-field ion source.

Saddle-field ion sources generally need to be maintained at pressures of 10^{-3} to 10^{-6} mbar (Franks, 1979, Sarangi et al, 2000). Such pressures limit undue scattering of the beam.

The energy of ions produced in the saddle field ion source are reasonably monoenergetic with an energy that is a fixed fraction of the applied anode potential (Harrold and Delchar, 1989). The ion beam current is dependent on the path length of the electrons oscillating about the saddle point. Therefore, to increase the ion current an increase in the cathode separation must be made. It is this feature that dictates the size of the saddle field ion source. The Saddle-Field Ion source of Franks, 1984 produces a beam covering a circular area with diameter of 7.5 cm. The source typically operates at 800 kV with a particle flux equivalent to 10 to 40 mA. The calculations performed in this study are based on these parameters and are easily achievable with Saddle-field ion sources.

Saddle-field ion sources can operate with three distinct discharge modes.

1. Oscillating mode_ Occurs at high voltage and low pressure and the discharge is anisotropic because of electrons oscillating in the vicinity of the symmetry axis of the structure. Electron space charge is not locally compensated by ion space charge. Probability of ionisation is high lending to high beam currents.
2. Glow discharge mode_ Occurs at relatively high pressure and low voltage and the discharge is isotropic and the electron space charge is locally compensated by ion space charge. Electron oscillation at the Saddle-field region is significantly prevented leading to a loss in ionisation efficiency and hence low relative beam currents.
3. Transition mode_ Occurs between the previously mentioned modes. The transition pressure is dependent on the geometry of the structure, the operating gas and the operating voltage.

(Godechot et al, 1990)

According to Muggleton, 1991, saddle field ion sources have advantages over other ion sources including

1. There is no filament and the device operates electrostatically; no magnetic field is used.
2. The electrical supplies are fairly simple and inexpensive (compared with duoplasmatron sources)
3. The source can be made small, is simple in construction and inexpensive to manufacture.
4. Requires minimum of technical expertise in ion beams to operate.

3.7 Sputter Process

3.7.1 Introduction

Sputtering is the phenomenon where atoms are removed from a solid surface due to energetic particle bombardment (Zalm, 1989). Sputtering was first observed in 1852 by Grove but it was not until the 1900's that the effect was found to be caused by ion bombardment. Sputtering has been extensively studied since and is now used to glean information about the interactions between ions and matter, for surface cleaning and etching, thin film deposition, surface and surface layer analysis and for producing ion sources (Wasa and Hayakawa, 1992). The importance of sputtering for this project concerns the integrity of the targets after helium-3 bombardment. Processes such as sputtering can significantly reduce target thickness and reduce target strength influencing the target lifetime and fluorine-18 yields as well as posing a possible safety issue concerning the Ultra High Vacuum (UHV) system.

3.7.2 Sputter Yield

Sputtering is quantified in terms of the sputter yield which is also known as the sputter coefficient. The sputter yield, S, is defined as the mean number of atoms removed from the surface of a solid per incident ion (Wasa and Hayakawa, 1992).

$$S = \frac{\text{atoms removed}}{\text{incident ions}} \qquad (5)$$

where: S = the sputter yield

The sputter yield can be determined empirically by the following methods:

1. Weight loss of target
2. Decrease of target thickness
3. Collection of the sputtered materials
4. Detection of sputtered particles in flight

The sputter yield is primarily dependent on the initial stopping power at the target surface and the binding energy of the target. These parameters can be affected by a number of factors of which the most dominant include:

1. Energy of incident particles
2. Projectile type
3. Target materials
4. Angle of incidence of incident particles
5. Crystal structure of the target surface

3.7.2.1 Ion Energy

Sputter yield is highly dependent on the incident ion's energy. The incident ion energy can be broken into three distinct regions in terms of sputter behaviour (Wasa and Hayakawa, 1992).

1. The threshold region (E < 100 eV)
2. Low energy region (100 eV < E < 10 keV)
3. High energy region (E > 10 keV)

Below a threshold energy sputtering will not occur. This is almost certainly related to the mechanism of sputtering and in 1962, Stuart and Wehner measured reliable threshold energies for various materials to be in the order of 15 to 30 eV (Stuart and Wehner, 1962). In the low energy region near the threshold the sputter yield is proportional to the square of the incident ion energy. This relation continues

until the incident ion energy is in the order of 100 eV. Above 100 eV the incident ions collide with the surface atoms of the target and the number of displaced target atoms is simply proportional to the incident ion energy (Wasa and Hayakawa, 1992).

3.7.2.2 Target Materials

The key target feature that affects sputtering is the surface binding energy. Before a particle is actually emitted from the target it must overcome the attractive binding forces of the surrounding material. For the case of an atom being sputtered it is often sufficient to assume a planar surface binding potential (Sigmund, 1981), which acts to reduce the velocity of the emitted atom perpendicular to the target surface. For molecular sputtering the binding can be significantly more complicated (Urbassek, 1992).

The atomic number and weight of the target atoms have a significant effect on the sputter yield. It has been shown that the sputter yield varies periodically with the target elements atomic number (Wasa and Hayakawa, 1992) with the yield increasing consistently as the D shells are filled. Periodicity is also observed with the sputtering thresholds.

The crystal lattice configuration of the target affects the sputter yield. Ordering within a lattice effectively shields subsurface atoms as they are directly behind surface atoms in the ions path. This reduces the likelihood of an ion colliding with the subsurface atoms and the ion is said to “channel” (Zalm, 1989). The magnitude of this decrease is dependent on the “width” and “acceptance angle” of a channel, which is determined by the density of atomic rows in the plane perpendicular to the ions path (Zalm, 1989).

Sputtering of multicomponent materials is of relevance to this project and has the feature of enrichment and depletion of surface layers due to sputtering compared to purely single element targets (Zalm, 1989). According to the Linear Cascade Model the energy and momentum during sputtering is dependent on the masses of atoms involved in the cascade. This results in different ejection probabilities for the different types of atoms of which the target is composed. This effect is dependent on the surface binding energies of the component atoms.

3.8 Stopping and Range of Ions in Matter (SRIM) Monte Carlo Program

3.8.1 Introduction

SRIM is a Monte Carlo software package that can be used to simulate the behaviour of energetic charged particles in matter. For this project SRIM was only required for stopping power calculations. SRIM calculates the stopping and range of ions (10 eV - 2 GeV /amu) into matter using a quantum mechanical treatment of ion-atom collisions. SRIM first became available in 1985 and has since been extensively updated. In particular, the stopping of relativistic light ions with energies above 1 MeV/amu has been improved and corrections have also been made as extensive new experimental data became available (Ziegler, 2004).

3.8.2 The Science of SRIM

In SRIM calculations, collisions between ions and target atoms are treated as coulombic interactions between the overlapping electron shells. The ion also has long range interactions with target atoms creating electron excitations and plasmons within the target. These are described in SRIM by including a description of the target's collective electronic structure and interatomic bond structure when the calculation is setup. The charge-state of the ion within the target is described using the concept of effective charge, which includes a velocity dependent average charge state and long range screening due to the collective electron sea of the target (Ziegler, 2004).

3.8.2.1 Stopping of Ions in Compounds

The stopping of ions in compounds is very important in the calculations of this project. In the upgrade to SRIM-2003 significant effort was made to improve the stopping calculations for ions in compounds. Traditionally, the stopping of ions in compounds was calculated according to Bragg's rule, where the stopping power of a compound is estimated by the linear combination of the stopping powers of its individual elements (Ziegler, 2004). Bragg's rule has been found to agree with experimentally measured stopping powers in compounds to approximately 20 %.

The inaccuracy of Bragg's rule is because the energy loss of electrons in a material depends on the detailed orbital and excitation structure of the matter and is not accounted for by a simple linear sum of individual stopping powers. Any differences between bonding in elemental materials and in compounds will cause Bragg's rule to become inaccurate (Ziegler, 2004).

SRIM utilises a more sophisticated development of Bragg's rule to calculate the stopping of ions in compounds called the Core-And-Bond (CAB) approach. The CAB approach assumes that the stopping of ions in compounds can be predicted using the superposition of the stopping due to the atomic "cores" and then adding the stopping corresponding to the bonding electrons (Ziegler, 2004). The core stopping is similar to Bragg's rule in that the stopping component of each atom in the compound is added linearly. The chemical bonds of the compound then contain the necessary stopping corrections based on the nature of individual bonds. SRIM uses the CAB approach to generate corrections between Bragg's rule and the compounds containing the common elements in compounds: hydrogen, carbon, nitrogen, oxygen, fluorine, sulphur and chlorine (Ziegler, 2004). These bonding corrections that are used in SRIM have been extracted from the stopping of hydrogen, helium and lithium ions in more than 100 compounds generated by experimental data from 162 experiments (Ziegler, 2004). Because for this project protons and helium-3 are the ions of interest, SRIM can deliver stopping power values with an accuracy of better than 2 % at the peak of the ion's stopping power curves (approximately 125 keV/u) (Ziegler, 2004).

The CAB approach provides significant improvement in stopping power accuracy compared to Bragg's rule, however, it does have its limitations. These limitations include:

1. Errors when calculating stopping powers for conducting materials. The data for the bond corrections in SRIM is predominantly based on experiments on insulating targets. For conducting targets there may be an error with the calculated stopping correction being too small because theoretically, band-gap materials are expected to have lower stopping powers then equivalent conductors because the small energy transfers to

target electrons are not available in insulators. The magnitude of this effect is still unknown.

2. The list of elements used for bonding corrections is incomplete. In particular the light elements of helium, neon, lithium, beryllium and Boron are missing. This is because of a lack in experimental data. No experiments have been performed on the stopping of ions into elemental helium and data on the other atoms is considered too sparse by the creators of SRIM for inclusion. The omission of heavier target atoms is less significant as experiments have shown that for compounds with heavier atoms the deviations from Bragg's rule disappear.

(Ziegler, 2004)

3.8.2.2 Stopping of High Energy Ions

The stopping powers of high energy (E > 1 MeV/amu) ions have many components that are accounted for in modern Bethe-Bloch theory (Ziegler, 2004). Modern approaches to Bethe-Bloch stopping are complex. In this approach two significant components are not well described by pure theoretical considerations and hence SRIM relies on empirical data (Ziegler, 2004): These components are firstly, the mean ionisation energy of the target and secondly, the shell corrections for the target. The mean ionisation energy of the target corrects for the quantised energy levels of the target electrons and also any target phase correction. The shell corrections for the target corrects for the Bethe-Bloch assumption that the ion velocity is much larger than the target electrons velocities. For SRIM this term is usually dealt with by detailed accounting of the particle's interaction with each electronic orbit in various elements. Both the mean ionisation energy and shell corrections are only dependent on target so they are assumed to be the same for both heavy and light ions (Ziegler, 2004).

When the target material is a compound rather than monatomic the stopping of charged particles is conventionally described by Braggs additivity rule which claims that the stopping cross section of an atom is independent of its chemical and physical environment (Sharma et al, 2004). This implies that the stopping cross section of a molecule is equal to the stopping cross sections of its constituent atoms.

Limitations to this rule are widely known but it has been found that for projectile speeds well above the stopping maximum, Bragg's additivity rule is obeyed (Sharma et al, 2004).

3.8.3 SRIM Accuracy

The accuracy of SRIM has steadily increased with each successive upgrade. Table 2 shows the statistical improvements in SRIM-2003's stopping power accuracy when compared to both experimental data and to SRIM-1998.

Table 2 Accuracy of SRIM stopping calculations (adapted from Ziegler, 2004)

	Approx. data points	SRIM-1998	SRIM-2003	SRIM-2003 (within 5%)	SRIM-2003 (within 10%)
H ions	8300	4.5%	4.2%	74%	87%
He ions	6500	4.6%	4.1%	76%	89%
Li ions	1400	6.4%	5.1%	72%	83%
Be-U ions	9000	8.1%	6.1%	58%	82%
Overall accuracy		6.1%	4.8%	69%	86%

Besides the stopping powers calculated by SRIM and other information from the literature the design of the system is required to provide the calculation geometry for determining the expected yield of fluorine-18. Such a calculation will be useful in determining the feasibility of using the $^{3}He(d,p)^{4}He$ reaction to produce fluorine-18 for PET applications

4. System Designs

The first step in creating a system for producing fluorine-18 for FDG synthesis via the $^{3}He(d,p)^{4}He$ reaction is to develop a design that can produce adequate amounts of fluorine-18. This can be satisfied with theoretical calculations of the fluorine-18 yield for a given design with the number of assumptions in the calculation minimised. Some thought is also given at this stage of practical issues to be considered, but this is not the primary focus and such issues are not considered in depth.

4.1 Practical considerations

In the process of designing a system for fluorine-18 production a number of practical issues must be considered. Such issues include, ease of use and maintenance, physical size of the unit, safety to operators, patients and the general public including the more specific radiation safety consideration.

4.1.1 Ease of Use

It is the intention that the system be used in a typical nuclear medicine department operating a PET scanner. Currently such a department has no personnel experienced with heavy-ion beam systems. Hiring extra technical staff provides additional complications so the system must be easily operated by a typical healthcare worker who has minimal technical training. In all likelihood the system would be operated by nuclear medicine technicians who start the machine, leave it to operate and then return at a later time to collect the product fluorine-18, synthesise it with FDG and then inject into the patient prior to PET scan. As such, the machine would need minimal user time to operate and would be stand-alone and not require the user to be present during operation.

4.1.2 Small size

An important aspect that will affect both the practical and economic feasibility of a system design is its size. The larger the size of the system the more it will cost in terms of infrastructure. A device of tabletop size could easily be accommodated in most nuclear medicine departments. A larger device that requires a dedicated room may prove more difficult to house and in some cases may need to be located away from the PET scanner necessitating transport of the fluorine-18 through the hospital. Dedicating a whole room for a device can be impractical for a hospital, especially if the room has special requirements such as shielding for radiation protection purposes.

4.1.3 Safety

To be accepted into clinical use in a nuclear medicine department the device must meet stringent safety standards. The safety of operators, patients, general staff and the public must be ensured. Electrical and mechanical safety must be ensured and as the device is based on nuclear reactions then radiation safety is a principal concern. Radiation exposure from the device must be kept to a minimum. This may require the addition of shielding to the design. The safe removal of activated by-products from nuclear reactions within the device is another radiation protection issue.

4.2 Economic considerations

The current method of producing fluorine-18 involves the use of a medical cyclotron that costs initially in the order of millions of dollars. The exact amount is dependent on infrastructure costs, which are unique in each case. A fluorine-18 generating system, designed to operate at an individual PET facility, will only be economically feasible if it is significantly cheaper than a centrally located cyclotron serving a number of PET facilities. This is because of the cyclotron's ability to produce large and varying amounts of FDG and its ability to produce other PET isotopes besides fluorine-18.

The cost of running the device once it has been commissioned is also important in determining the feasibility of a design. Maintenance and repair costs need to be minimised as well as the use of input materials. An important factor here concerns the availability of the required input materials. The device requires exotic materials such as deuterium, oxygen-18 and helium-3 and the availability of such materials largely determines their cost.

4.3 Yield Efficiency

The design of a feasible system is largely dependent on the fluorine-18 yield efficiency of the system. If the system is capable of producing large quantities of fluorine-18 quickly, easily and for minimal input resources then the system will be more effective. FDG dosage is dependent on the patient's weight with an average sized patient requiring about 440 MBq (Paul Cardew, Chief Nuclear Medicine Physicist, John Hunter Hospital, Newcastle, NSW, Australia. private communication). This equates to a 55 kg patient when the general rule of 8 MBq/kg of Everaert et al, 2003 is applied. 440 MBq will subsequently be used as an approximate representative single patient dose in calculations. Based on this, to treat five average sized patients per day at one hour intervals and accounting for estimated losses the system would be required to produce about 6.5 GBq per day.

4.4 Designs

To determine feasibility of the system fluorine-18 yield calculations were performed on two separate designs that could possibly meet the practical and economic considerations already outlined.

4.4.1 Deuterated Solid Target

The first design followed the most obvious method of placing a solid deuterium enriched target in the helium-3 beam. A second film, enriched with oxygen-18, is then placed on the far side of the deuterated target. With the helium-3 beam incident on the deuterated target, energetic protons would be produced via the $^{3}He(d,p)^{4}He$ reaction. A large proportion of these protons would exit the deuterated

target in the direction of the oxygen-18 target where fluorine-18 could be produced following the $^{18}O(p,n)^{18}F$ reaction. This process is illustrated in figure 10.

The great advantage of this design is that it resembles the medical cyclotron method of producing fluorine-18 except that the source of the proton beam has changed. This means that once the proton beam has been produced via the $^{3}He(d,p)^{4}He$ reaction, the same H_2O^{18} (heavy water) oxygen-18 target and fluorine-18 extraction system can be used as with a medical cyclotron. This would allow some existing systems already used with cyclotrons to be utilized.

The deuterated target in this design performs two roles. Firstly, it acts as the source of deuterium for the $^{3}He(d,p)^{4}He$ reaction and secondly it acts as the barrier between the vacuum, which is required for the helium-3 beam, and the atmospheric pressure at which the heavy water oxygen-18 target is kept. This design allows for easy extraction of the fluorine-18, as the vacuum need not be breached. Because of the multiple role of the deuterated target, the choice of material is important. A material is required that has the following characteristics:

- sufficient structural integrity to act as a vacuum seal
- must not out-gas under vacuum
- must retain structural integrity under ion bombardment
- must conduct heat relatively well
- must normally have a high hydrogen content to maximise the deuterium concentration upon deuteration
- must be able to be supplied with hydrogen in isotopic deuterium form at a reasonable price.
- Must have all the above properties while also being thin enough to allow the transmission of the 18 MeV proton beam without significant energy loss.

A number of target materials were investigated. The conventional target material used in medical cyclotrons is Havar. Havar was not investigated in this project because no supplier could be found of Havar in the deuterated form. A principal difficulty was the availability of deuterated materials at reasonable prices.

The first target material investigated was zirconium deuteride with which Horn et al (1995) had conducted experiments on the $^{3}He(d,p)^{4}He$ reaction. This material has been demonstrated by Horn et al to meet the requirements for this project but the difficulties in obtaining Zirconium (because it is classified as a restricted nuclear material) meant that it was not pursued for this project.

During the investigation into deuterated targets a supplier in Montreal, Canada named Polymersource Inc (www.polymersource.com) was found that could supply a large variety of plastics in either partially or completely deuterated form. From the deuterated plastics available through Polymersource Inc, deuterated Mylar ($C_{10}D_8O_4$) was chosen for further examination. Mylar has a number of characteristics required for the target material including a high deuterium concentration of 8 deuterium atoms per molecule yielding 3.37 x 10^{28} deuterium atoms per cubic metre. Mylar is also commonly used in UHV applications as it does not out-gas and has good structural integrity. Besides vacuum applications the properties of Mylar are also well understood under ion bombardment. This feature is useful as it allows easy prediction of the Mylar degradation and heat conduction properties under bombardment from the helium-3 beam.

The deuterated Mylar supplied from Polymer source Inc is sold at US$600 per gram (as of October 2005). Based on a target of dimensions 250 cm^2 by 1 mm thick as is used for calculations it is envisaged that about 35 g per target is required. Such a target would cost US$21000 and is thus prohibitively expensive.

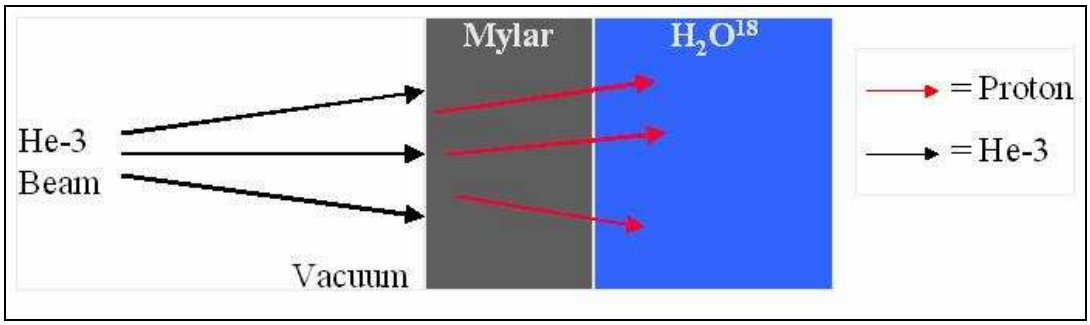

Fig 10 Schematic diagram of the deuterated target design (not to scale).

After the Mylar target, the system is similar to that of a Medical cyclotron in that a proton beam of megavoltage energy is incident on an oxygen-18 heavy water

target, although there are some differences in the proton beam compared to a medical cyclotron beam, especially in terms of the beam quality and current. A principle difference is that the cyclotron protons are in the form of a narrow, well-defined beam while for the deuterated solid system the protons are emitted quasi-isotropically from the $^{3}He(d,p)^{4}He$ reaction. The useable proton beam emerging from the Mylar will be broad and ill-defined. With these differences in the proton beam it may be necessary to alter the design of the heavy-water target from the medical cyclotron target design. In all likelihood the dimensions of the target would need to be increased and the calculations performed in this project assume this. Such a broad target design is well suited to a saddle field ion source, which are principally area sources. Assuming only minor adjustments need to be made to the heavy-water target apparatus used in medical cyclotrons then the basic design can be used in this deuterated polymer target system

4.4.1.1 Alternative Plastics to Mylar

The SRIM software includes a library of target materials that include a range of plastics from which stopping powers can easily be calculated and hence be easily used to replace Mylar in the fluorine-18 yield calculations. The hydrogen concentration in a range of plastics in this library were compared to Mylar to determine whether a suitable material could be found with a higher deuterium concentration. This would make a more efficient target for proton production via the $^{3}He(d,p)^{4}He$ reaction. The results of this investigation are summarised in table 3.

Table 3 Potential Deuterium concentrations of selected plastics assuming 100% deuteration.

Plastic	**Deuterium Concentration (D/m^3) ($x10^{28}$)**	**Deuterium concentration relative to Mylar (%)**
Mylar	3.36	100
Lucite	5.35	159
Paralene-n	4.77	142
Plexiglas	6.12	182
Bakelite	4.92	146

Epoxy	2.95	88
Formvar	5.84	174
Lexan	2.16	64

The calculation of hydrogen/deuterium concentration summarised in table 3 shows that Mylar has a relatively low concentration of hydrogen/deuterium to other plastics investigated. The highest concentration was found in Plexiglas acrylic ($H_6C_4O_2$) at 6.12 x 10^{28} deuterium atoms per cubic metre. This equates to 1.82 times the concentration of deuterium in Mylar.

4.4.2 Super heavy water Target

The second design combined a target for proton generation with a target for fluorine-18 production, which contains both deuterium and oxygen-18. This is achieved using a super heavy water target where both the hydrogen and oxygen atoms have extra neutrons in the nucleus to form the molecule D_2O^{18}. This design is shown schematically in figure 11.

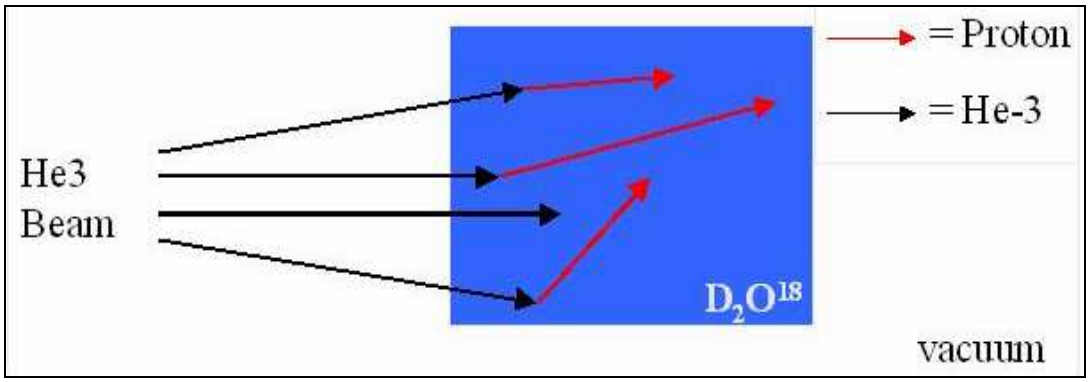

Fig 11 Schematic diagram of the super heavy water target design (not to scale).

The advantage of this design is that both the deuterium and oxygen-18 concentrations are maximised as there are no additional non-essential atoms in the target, such as carbon and oxygen-16 in the Mylar that are not used for either the $^3He(d,p)^4He$ or the $^{18}O(p,n)^{18}F$ reactions. Additionally, as soon as the $^3He(d,p)^4He$

reaction has taken place the product protons are in the vicinity of oxygen-18 atoms so that the $^{18}O(p,n)^{18}F$ reaction can take place. This has two advantages;

- Firstly, more protons are exposed to oxygen-18 and have the chance to react provided that the super heavy water target has dimensions larger than the protons pathlength in water. Approximately half of the protons will still escape the system. This is because of the small helium-3 range in water (5.31 μm), which means that the $^{3}He(d,p)^{4}He$ reactions will take place near the front surface of the super heavy water target. This is still geometrically advantageous compared to the Mylar target system where the protons are produced outside the heavy-water target.
- Secondly, the protons have no energy loss before they come into the vicinity of oxygen-18 atoms so they have the opportunity of reacting over their entire pathlength. This is advantageous over the deuterated target system where protons must traverse the majority of the Mylar target thickness, with associated energy loss, before reaching the heavy water.

The disadvantages associated with the super heavy water system relate to the practicalities of using a target which is liquid at room temperature. Firstly, there is a difficulty in containment of the super heavy water under UHV and stability so that the helium-3 beam can be targeted onto it. A solution to this problem is to freeze the super heavy water target. Super heavy water has essentially similar chemical properties to ordinary water and as such has melting point at 0 °C. For such a melting point freezing the super heavy water should pose few difficulties, however, under helium-3 bombardment it can be expected that significant temperature increases will occur.

Another major impracticality with the super heavy water design revolves around the feature of having the frozen super heavy water target situated completely in the vacuum. This design feature is proposed so that no vacuum seal material is required between the helium-3 beam and the target, which will inevitably attenuate the helium-3 beam similar to the Mylar attenuating the product protons in the

deuterated target design. Having the super heavy water target under vacuum provides difficulties in extracting the product fluorine-18 and a higher level of technical expertise would be required for the system operator, as they would need to be competent at operating vacuum systems.

A producer of super heavy water in Israel has been found that can supply super heavy water through the Australian supplier, Novachem Ltd. The Novachem super heavy water is produced with 90 to 95 % of the hydrogen component as deuterium and 95 % of the oxygen component in the form of oxygen-18, and can be bought for $US115 per gram plus delivery and GST. Delivery charge is set at $US75 plus GST per order and the super heavy water is supplied in 10 gram amounts. In the design used for yield calculations a 10 cm^2 by 0.4 cm deep super heavy water target is used to maximise the helium-3 beam target area and provide sufficient target depth to cover the product proton's pathlength in water. Such a target has mass of approximately 4 grams which means that a single minimum supply of super heavy water would provide two targets with approximately 2 grams surplus (for any losses in the freezing process for example). This would cost $US1237 and includes shipping costs.

Now that system designs have been theorised such that geometries for calculations are available and calculation requirements such as stopping powers are available via SRIM the calculation methodology can be investigated for calculating the yields of fluorine-18.

5. Calculations

5.1 Introduction

To determine whether the systems were feasible for fluorine-18 production, calculations were performed to predict the yields of fluorine-18 produced. Such a yield is determined by the specific features of the target arrangement and the saddle-field ion source.

There are multiple steps involved in calculation of the yield of fluorine-18 and other by-products. This chapter describes the processes that were considered and their methods of calculation. The following are considered explicitly:

The production of protons from the ^{3}He(d,p)^{4}He reaction. This includes the energy and angular distribution relative to the direction of an incoming helium-3 beam, the ion beam current and deuterium concentration in the target.

The conversion of Oxygen-18 to Fluorine-18. This includes consideration of the geometry of irradiation, proton attenuation, the interaction of slowing-down protons with oxygen-18, subsequent decay of oxygen-18, loss of protons through other interactions and other interactions arising from decay products.

Determination of system utility. These processes are considered for the two system designs being considered. For each, the loss of target material by sputtering and/or loss of target nuclei are considered to enable determination of expected useful yields of fluorine-18 with time.

5.2 Nuclear Reaction Product Yield Calculations

The yield of product particles and daughter nuclei from an ion-induced nuclear reaction can be calculated using equation 5:

$$Y = N_o C_T \int_{path} \sigma(E) dx$$

which, for a discretely defined energy spectrum becomes:

$$Y = N_o C_T \sum \sigma(E) \delta x \qquad (5)$$

where: Y = number of product particles yielded
N_o = number of incident ions
C_T = concentration of target parent nuclei (atoms/m^3)
$\Sigma\sigma(E)\delta x$ = total integrated cross section over the incident ion's path length (m^3)

To calculate the final yield of fluorine-18, equation 5 must first be used to calculate the expected yield of protons from the $^3He(d,p)^4He$ reaction. This yield is then used as the number of incident ions, N_o and equation 5 is used again to calculate the yield of fluorine-18 from the $^{18}O(p,n)^{18}F$ reaction. This assumes negligible contributions from reaction products to other subsequent reactions. The calculations are performed along the path of particles as they slow down, without consideration of angular deflection along the path. These 'pathlength' calculations are then considered in the context of a three dimensional calculation as the number of incident ions is based on beam currents per unit area from area ion sources.

5.2.1 Proton Yield

The first step in the calculation is to determine the expected proton yield due to ion irradiation. The proton yield is dependent on the energy and current of the incident helium-3 beam and the composition of the deuterium-loaded target. The former is a function of the helium-3 ion source.

5.2.2 Helium-3 Current

A 1 MeV helium-3 beam at current of 100 mA was used for calculations as these parameters were found to maximise the fluorine-18 yield while still lying easily within the operational capabilities of ion sources in the literature (Franks,

1984, Keller, 1989). At 1 MeV, singly charged helium-3 atoms impinging on the target at 100 mA correspond to 100 kW of power. This is significant in that such energy transfer will result in significant heating of the target resulting in thermal defects that could affect the target lifetime, durability and hence practicality of the system.

The helium-3 beam current is used to calculate the rate of incident ions in equation 5 with the assumption that all helium-3 are only singly ionised.

5.2.3 Concentration of Deuterium and the total Integrated Cross section

As it has been chosen to accelerate the helium-3 then it is the deuterium atoms that become stationary in the laboratory reference frame. The concentration of target nuclei term in equation 5 is thus the concentration of deuterium. This parameter is dependent on the target material utilised with each system design. The atomic density of deuterium was calculated from the molecular density. Such a calculation assumes 100 % target purity and that 100 % of the hydrogen present in the target is deuterium. The unit of deuterium concentration used in calculations is atoms/m^3.

As a charged particle moves through a medium it loses energy. This change in energy results in variation in the probability that the helium-3 nucleus will fuse with a deuterium nucleus due to the change in the reaction cross section with energy. This phenomenon is evident in figure 8. The total integrated cross section is the summation of the $^3He(d,p)^4He$ cross section over the helium-3 path-length in the deuterated medium.

5.2.3.1 Helium-3 Stopping-Power

To determine the total integrated cross section, the first step is to determine the likely helium-3 kinetic energy at every point along its pathlength through the deuterated medium. To establish this, stopping powers (this is incorrectly referred to as a stopping power in the literature whereas it is more correctly termed a stopping force (http://www.icru.org/n_002_7.pdf). In this work the more common term will be used to conform to literature convention and avoid confusion) of the helium-3 in

the medium are required. Stopping powers are defined as the rate of kinetic energy loss per unit path length of the particle (dE/dx) (Khan, 2003).

For the purpose of these calculations, stopping powers were determined using the SRIM Monte Carlo simulation program (Ziegler, 2004). Once the stopping powers have been calculated the typical energy of a helium-3 ion in the deuterated target can be determined at every point along its pathlength. For calculation, the pathlength is divided into small incremental lengths (dx) and the stopping powers are converted into units of keV/dx. At any point along its pathlength the helium-3 ions have a mean energy defined by equation 6. Not all the particles will have this exact energy, but there will be a spread in energy defined by the energy straggling which is small and will not impact on the calculations significantly. This method is known as the Continuous Slowing Down Approximation (CSDA)

$$E_i = E_0 - \sum_i \left(\frac{dE_i}{dx} \right) dx_i \qquad \text{until } E_i = 0 \qquad (6)$$

where: E_i = the ion energy
E_0 = the initial ion energy
$\frac{dE_i}{dx}$ = the stopping power at energy E in the medium
dx_i = the incremental length

In the simulation below it was assumed that at the surface of the target the helium-3 ion has kinetic energy of $E_0 = 1$ MeV. For the calculations the incremental length was chosen to be 10 nm. This value was chosen to provide adequate sampling of the particles energy over its pathlength. The values for helium-3 stopping powers in deuterated Mylar and super heavy water (H_2O^{18}) as determined using SRIM are presented in figure 12.

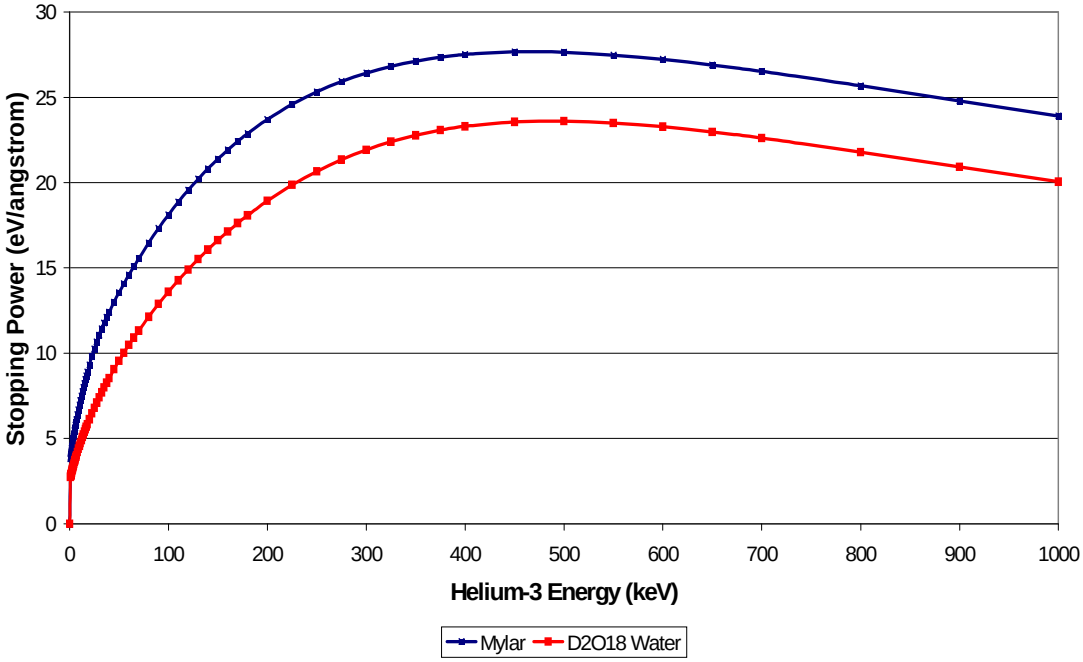

Fig 12 Helium-3 Stopping Powers in Mylar and super heavy water as produced by SRIM

5.2.3.2 $^{3}He(d,p)^{4}He$ Reaction Cross sections

By assigning the $^{3}He(d,p)^{4}He$ reaction cross sections of figure 8 to the table of the ion's energy at each incremental depth in the target material a table of reaction cross section versus particle position along its pathlength is produced. If all the cross section values in this table are summed and then multiplied by the length of the incremental depth the value for the total integrated cross section is determined.

When the total integrated cross section is multiplied by the concentration of deuterium and also by the rate of incident helium-3 ions then the rate of proton production is determined.

5.3 Fluorine-18 Yield

Once the rate of proton production is determined it can be used as input in calculating the rate of fluorine-18 production via the $^{18}O(p,n)^{18}F$ reaction by once again using equation 5.

5.3.1 Useable Proton Current

The proton yield per second is used as the rate of incident ions in equation 5 for the fluorine-18 yield calculation. Because the helium-3 particles have range of only a few micrometers in the deuterated targets (4.3 μm in Mylar and 5.32 μm in D_2O_{18} at 1 MeV, SRIM, 2003) this means that protons are produced right at the front edge of the deuterated targets. This fact combined with the quasi-isotropic distribution of protons from the $^{3}He(d,p)^{4}He$ reaction means that some protons will be emitted out of the oxygen-18 target and hence not be available for the $^{18}O(p,n)^{18}F$ reaction. Because the protons are produced at the edge of the deuterated target approximately half the protons will enter the target and hence transmit through the target to be incident on the oxygen-18 target. Hence, for calculations, the value for the rate of incident ions used in equation 5 for the $^{18}O(p,n)^{18}F$ reaction utilised a fraction of the proton yield for the $^{3}He(d,p)^{4}He$ reaction for both the deuterated Mylar system and the super heavy water system. The fraction of protons utilised is dependent of the geometry of the system which is illustrated in figure 13.

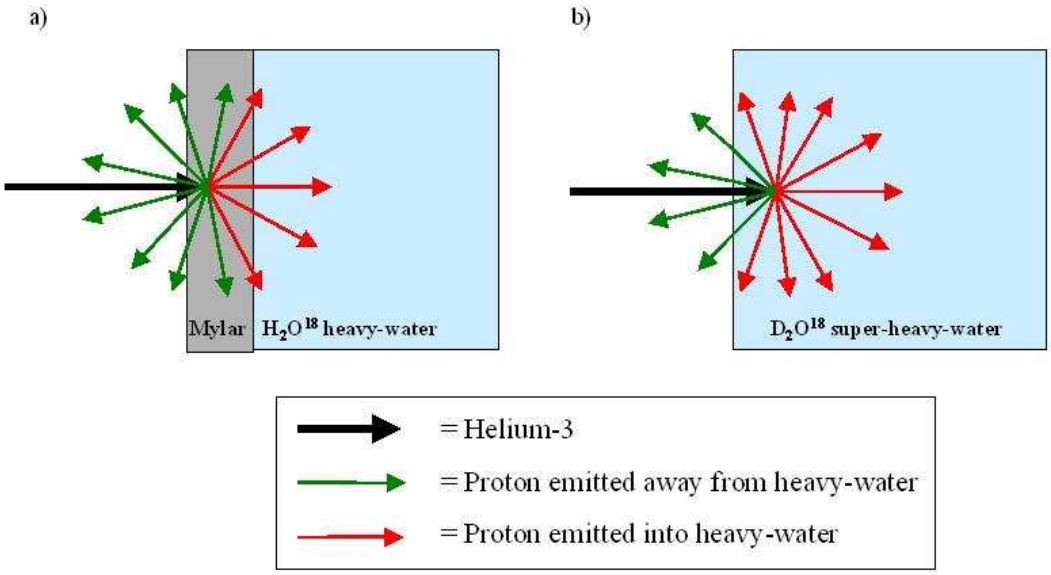

Fig 13 Diagram illustrating the proportion of protons generated by the $^{3}He(d,p)^{4}He$ reaction in a) the deuterated Mylar system and b) the super heavy water system that travel through the oxygen-18 water and can initiate the $^{18}O(p,n)^{18}F$ reaction. The red arrows depict protons that travel through the heavy-water. The green arrows denote protons that have minimal or contact with the heavy water. Diagram not to scale.

Figure 13a shows that for the deuterated Mylar system Less than half the protons produced will travel into the heavy water. Using the initial Mylar thickness before sputtering of 1 mm and the proton range in Mylar of 2.61 mm as calculated using SRIM it was determined using simple geometry that approximately 37.2 % of the protons produced travel into the heavy-water. This assumes that the production of protons via the $^{3}He(d,p)^{4}He$ reaction is completely isotropic. The small helium-3 range in Mylar (4.3 μm from SRIM) is also accounted for but has negligible effect. Thus 37.2 % of the protons produced via the $^{3}He(d,p)^{4}He$ reaction are useable for the $^{18}O(p,n)^{18}F$ reaction.

Figure 13b shows that for the super heavy water system, the assumption that half the protons generated will travel into the super heavy water is an under estimation. This is because there is no Mylar for the protons to traverse before coming into contact with the super heavy water and also because the helium-3 typically travels a small distance into the super heavy water before reacting with the deuterium in the $^{3}He(d,p)^{4}He$ reaction. If this distance were zero (ie the helium-3 reacted right at the surface of the super heavy water) then the assumption that half the protons generated will travel into the super heavy water would be true neglecting the negligible losses due to protons scattering out of the super heavy water. As the distance is small (maximum of 5.32 μm, SRIM, 2003) then the assumption is still valid.

5.3.2 Helium3 and Proton Losses

The useable proton current assumes that all protons produced are available for the $^{18}O(p,n)^{18}F$ reaction. However, some protons may be involved in other nuclear reactions in which case they would be unavailable for the $^{18}O(p,n)^{18}F$ reaction. Such reactions could occur in both:

- The Mylar before the protons even come into contact with oxygen-18. In this case the possible reactions could be between protons and deuterium, oxygen-16 and carbon-12.
- The heavy water possibly between protons and hydrogen or deuterium. Such reactions would be in competition with the $^{18}O(p,n)^{18}F$ reaction and hence

act to lessen the yield of fluorine-18. It is also possible that there are other reactions between protons and oxygen-18 that do not produce fluorine-18 and such reactions will also work to minimise fluorine-18 yield

The possible loss of protons due to competing nuclear reactions also applies to the helium-3 beam. Any losses of helium-3 will lead to a loss of protons and hence loss of fluorine-18 yield. For calculation purposes possible reactions that could cause loss of helium-3 or protons were investigated and equation 5 was used to calculate the magnitude of such loss.

The products of the unwanted reactions could also pose practical problems. It is possible that the product atoms could:

- Decrease the structural integrity of the deuterated plastic target
- Have large total reaction cross sections with helium-3 or protons further minimising the helium-3 or proton beam currents
- Be radioactive or toxic making the targets hazardous to handle.

For both systems the potential losses due to unwanted nuclear reactions were investigated. A large number of such reactions were found between the relevant particles and nuclei to this project. However, reactions were ignored that had: threshold energies higher than the energy ranges applicable to this project, cross sections of order less than 1 mbarn in the relevant energy range (as such cross sections are small compared to the hundreds of mbarn associated with the $^{3}He(d,p)^{4}He$ and $^{18}O(p,n)^{18}F$ reactions) or those reactions that could not be investigated due to lack of cross section data in the relevant energy range. In a small number of cases linear interpolation was used to estimate cross section data for energy ranges between two data sets where it seemed appropriate to do so.

5.3.3 Concentration of Oxygen-18 and the Total Integrated Cross Section

The concentration of oxygen-18 was calculated in the same manner as the concentration of deuterium concentration mentioned previously for the proton yield calculation.

The total integrated cross section for the $^{18}O(p,n)^{18}F$ reaction is determined as for the $^{3}He(d,p)^{4}He$ reaction. The stopping powers of the protons in the oxygen-18 target are calculated using SRIM and presented in figure 14 and the cross section values are those presented in figure 5. One major difference between the total integrated cross section calculations for the $^{3}He(d,p)^{4}He$ reaction and the $^{18}O(p,n)^{18}F$ reactions involves the initial incident ion energy. For the $^{3}He(d,p)^{4}He$ reaction the initial incident ion energy is simply the energy of the helium-3 ion as it leaves the ion source. Derivation of the initial proton energy is as straightforward as the protons are the product of a nuclear reaction and hence their initial energy must be calculated from first principles.

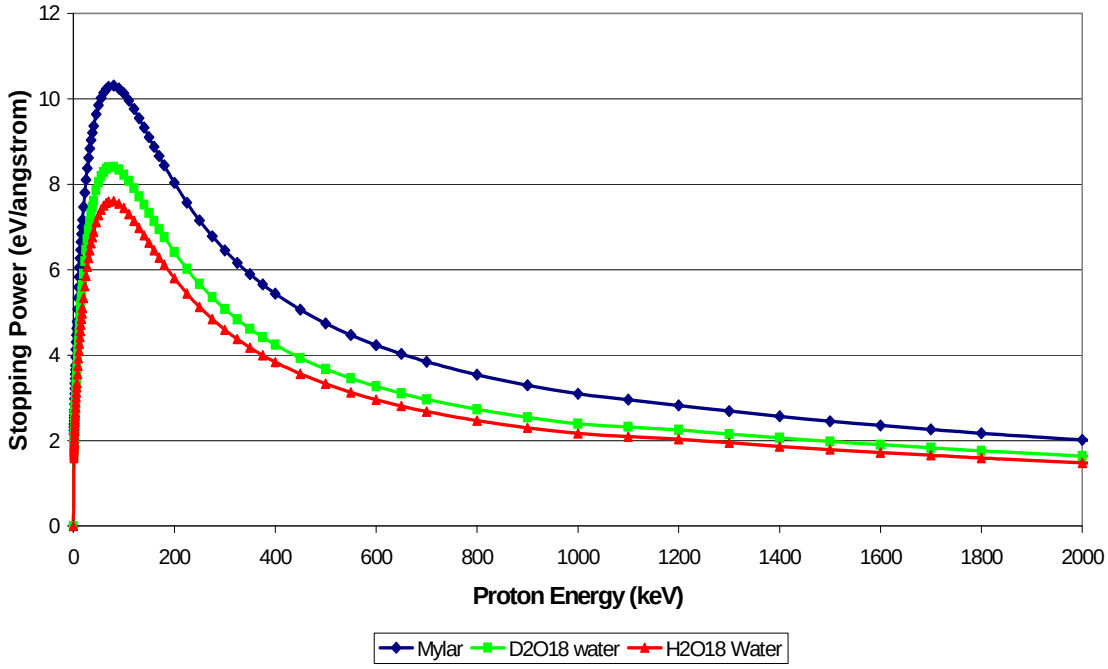

Fig 14 Proton stopping powers in Mylar, H_2O^{18} water and $D_2O^{!8}$ water as produced by SRIM.

5.3.4 Proton Initial Energy Calculations

The initial energy of the protons from the $^{3}He(d,p)^{4}He$ reaction is required in order to calculate the total integrated cross section in the $^{18}O(p,n)^{18}F$ reaction. The energy given to particles following a nuclear reaction is distributed such that momentum and energy is conserved. The total energy that is distributed is the sum of the initial particle energies before the reaction and the Q-value of the reaction,

which is the total mass of particles after the reaction minus the total mass of particles before the reaction multiplied by the speed of light squared according to Einstein's mass-energy relationship (equation 2). The distribution of this energy between particles following the reaction is governed by conservation of momentum and specifically by mass and direction of emission. To calculate the particle energies from a reaction it is convenient to convert to the centre of mass (COM) frame of reference to calculate the particle energies after reaction and then convert back into the laboratory frame of reference. This method simplifies the handling of conservation of momentum as it is implicit in the COM frame. The details of how such a calculation is performed are now presented.

With the Q-value of 18.35 MeV (Geist et al, 1999) for the $^{3}He(d,p)^{4}He$ reaction it is possible to calculate the product helium-4 and proton energies given the initial helium-3 energy. The reaction is presented schematically in figure 15.

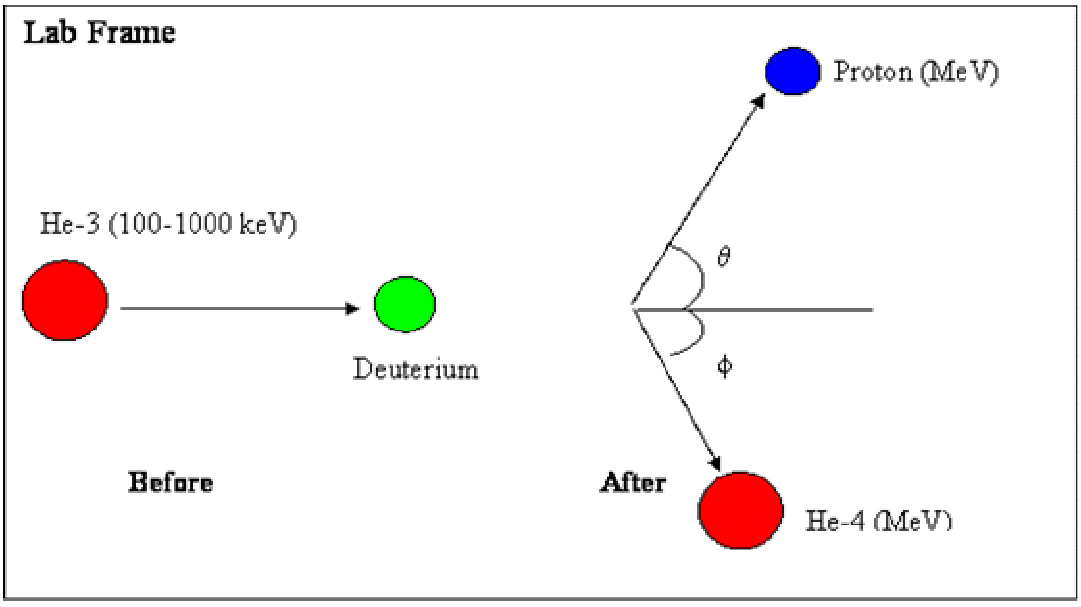

Fig 15 Schematic diagram of the $^{3}He(d,p)^{4}He$ nuclear fusion reaction in the laboratory frame of reference.

To calculate the kinetic energy of the proton as a function of direction of emission, the initial situation was transformed to the centre of mass reference frame in which the states of the final products of the nuclear reaction can be calculated from conservation of momentum and energy release, and more easily converted back to the laboratory frame.

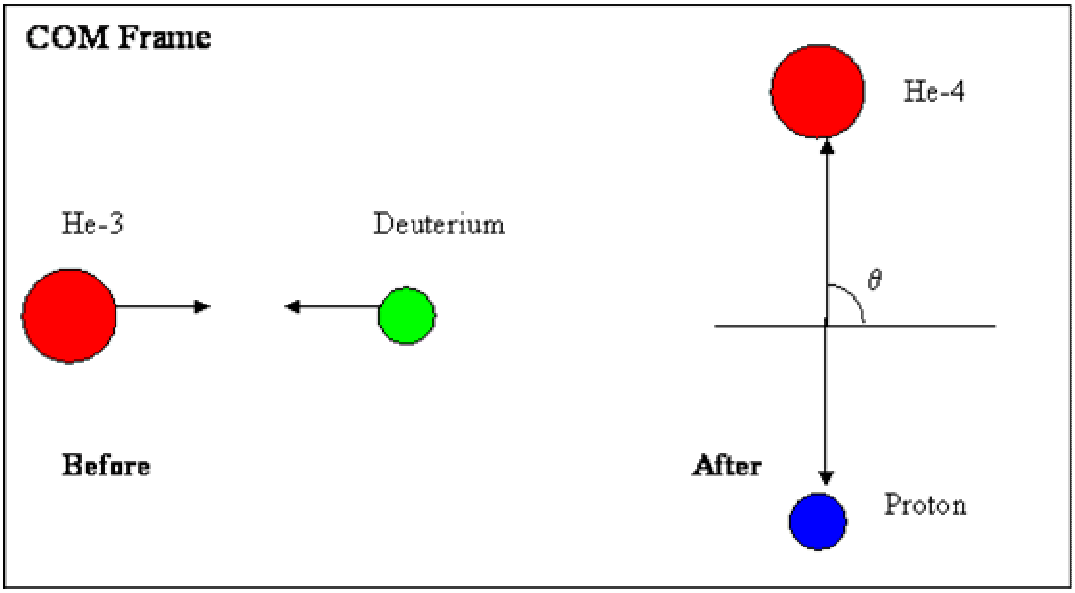

Fig 16 Schematic diagram of the $^{3}He(d,p)^{4}He$ nuclear fusion reaction in the Centre of Mass frame of reference.

To convert to the COM frame of reference the first step is to determine the centre of mass velocity, kinetic energy and momentum relative to the laboratory frame. On the assumption that the target atom is initially stationary this is performed using equations 7, 8 and 9:

$$v_{COM} = v_1 . \frac{m_1}{m_1 + m_2} \qquad (7)$$

$$KE_{COM} = KE_1 . \frac{m_2}{m_1 + m_2} \qquad (8)$$

$$P_{COM} = P_1 . \frac{m_2}{m_1 + m_2} \qquad (9)$$

where: v_{COM} = the velocity of the COM frame relative to the laboratory frame
v_1 = the velocity of the helium-3 nucleus in the laboratory frame
KE_{com} = the kinetic energy of the COM frame

KE_1 = the kinetic energy of the helium-3 nucleus in the laboratory frame.
P_{com} = the momentum of the COM frame relative to the laboratory frame.
P_1 = the momentum of the helium-3 nucleus in the laboratory frame.
m_1 = the mass of the helium-3 nucleus
m_2 = the rest mass of the deuterium nucleus

As the kinetic energy and the energy release is much less than the rest masses of the participating species, it is not necessary to use relativistic equations for this analysis. In the COM frame the momentum of the two product particles is equal and opposite both before and after the reaction. To find what this momentum is the first step is to determine the total kinetic energy after the reaction in the COM frame, which is found using equation 10.

$$KE_{COM}^{Total} = KE_{COM} + Q \quad (10)$$

where: KE^{total}_{COM} = the total kinetic energy in the COM frame after the reaction
KE_{com} = the kinetic energy of the particles in the Com frame before the reaction.
Q = the energy released in the fusion reaction

From this total kinetic energy, the product particles' momentum in the COM frame, which is equal and opposite for both particles in a two body system can be determined using equation 11.

$$P_{COM}^{total} = \sqrt{\frac{2.KE_{COM}^{total}}{\left(\frac{1}{m_3} + \frac{1}{m_4}\right)}} \quad (11)$$

where: P^{total}_{COM} = the product particles momentum in the COM frame after the reaction.
m_3 = the rest mass of the proton
m_4 = the rest mass of the helium-4 nucleus

By transforming now back to the laboratory frame the product particles' momentum in the COM frame can be used to determine the momentum of the individual particles in the laboratory frame. The relationships between momentum in the COM frame and the laboratory frame are presented in equations 12 and 13.

$$P_3 \sin\theta_3 = P_{COM}^{total} \sin\theta_{COM} \qquad (12)$$

$$P_3 \cos\theta_3 = P_{COM}^{total} \cos\theta_{COM} + m_3 v_{COM} \qquad (13)$$

where: θ_3 = the angle of emission of the particle in the laboratory frame
θ_{COM} = the angle of emission of the particle in the COM frame
3 = product particle from the reaction so can denote either the proton or helium-3 nucleus.

Calculations are performed over a range of θ_{COM} so that equations 12 and 13 have only two variables, P_3 and θ_3. The Kinetic energy of the product particles can easily be calculated from their momentum using equation 14.

$$KE_3 = \frac{(P_3)^2}{2m_3} \qquad (14)$$

It should be noted that the Q value for the ^{3}He(d,p)^{4}He reaction is found to be 18.89 MeV and the incident helium-3 energy ranges between 100 to 900 keV. This gives a combined total kinetic energy for the system between 18.99 and 19.79 MeV.

The resulting kinetic energies for both the proton and helium-4 nucleus are presented in figure 17 over a helium-3 energy range of 100 to 1000 keV. Of interest is the fact that the proton and helium-4 energies are not constant with varying COM emission angles. Results are presented for both COM angles of 0 and 90 degrees. This choice of angles represents the greatest variance in proton energy for which protons can be incident on the oxygen-18 target.

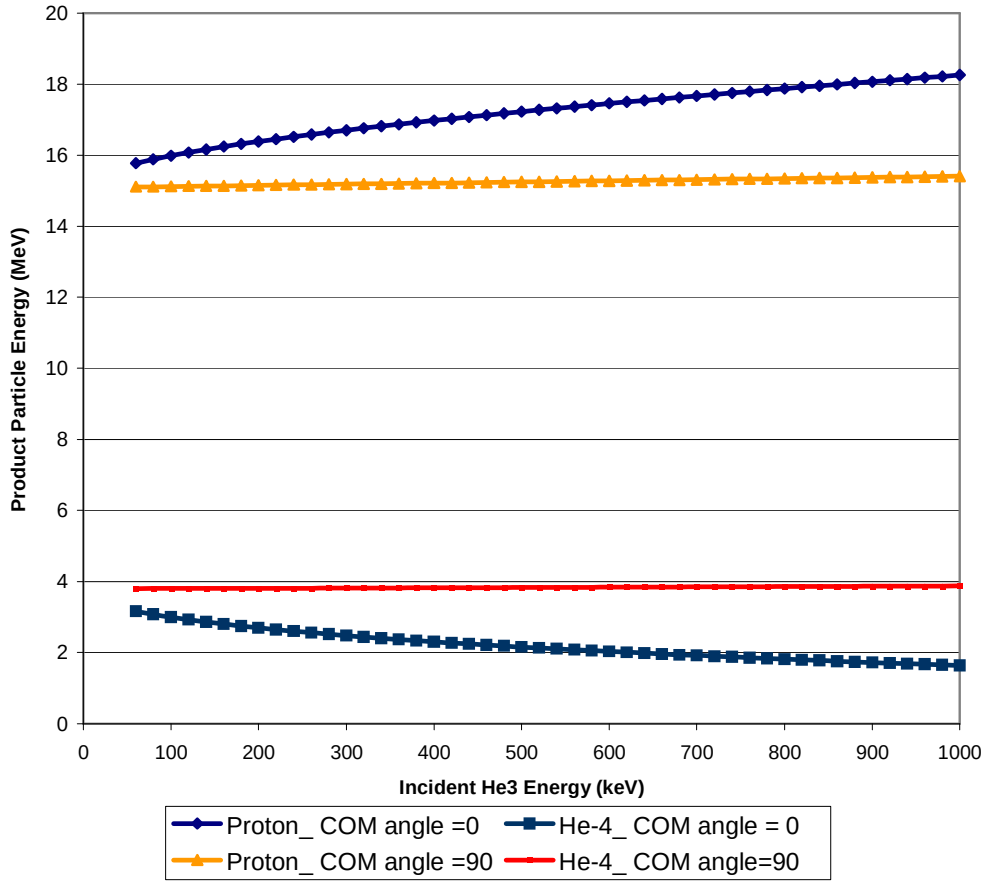

Fig 17 Calculated proton and helium-4 energies for both 0 and 90 degrees emission angle in the COM frame from the $^{3}He(d,p)^{4}He$ reaction. Product particle energy is plotted against input helium-3 energy.

The most important feature of figure 17 for these calculations is that the proton energy ranges from approximately 15 MeV to approximately 18 MeV in the helium-3 energy range of 100-1000 keV. It is interesting to note that the product helium-4 nuclei can have kinetic energy up to 4 MeV from the reaction and will cause damage (mainly electronic) to the target.

As incident helium-3 energy is increased the proton energy at COM angle of zero increases linearly, while the energy of the helium-4 nucleus emitted in the opposite direction drops linearly with incident helium-3 energy. This phenomenon is a result of the increase in initial momentum of the system before the reaction due to the increased helium-3 velocity. Hence, relative to the laboratory frame the COM frame has greater velocity and when the reaction takes place and the helium-4 and

proton are emitted in opposite directions (in the COM frame) the increase in COM frame velocity adds to the proton energy and subtracts from the helium-4 energy.

At 90 degrees emission angle in the COM frame the proton and helium-4 energies increase so slowly with increased incident helium-3 energy that they are almost constant. This is because at 90 degrees emission angle (COM) both the proton and helium-4 are moving almost perpendicular to the incident helium-3 nucleus. Any increase in helium-3 momentum will only have a small effect on the product particle's energy. The reason why both the helium-4 and proton both increase slightly in energy is because at 90 degrees emission angle in the COM frame both particles have a small forward component in the laboratory frame.

At the helium-3 energy of 1000 keV chosen for calculations figure 17 shows proton energies produced ranging between 15.35 and 17.87 MeV. For the purpose of calculation, these energies were averaged and hence an initial proton energy of 16.61 MeV was used for the total integrated cross section calculations for the $^{18}O(p,n)^{18}F$ reaction.

5.3.5 Fluorine-18 yield calculation

Similar to the proton production rate, the rate of fluorine-18 production is found by multiplying the total integrated cross section by the concentration of oxygen-18 in the target and by the proton production rate as in equation 5. For the purposes of PET scans the amount of fluorine-18 required is measured in terms of activity. Fluorine-18 has a half-life of 110 minutes (Krane, 1988). This gives a decay constant of 1.0519×10^{-4} s^{-1}. Using the calculated fluorine-18 production rate and accounting for radioactive decay with the use of the decay constant, the number of fluorine-18 atoms available after any period of helium-3 irradiation time can be calculated. By multiplying this number by the decay constant, the activity of fluorine-18 can then be determined. For a typical ^{18}FDG whole body PET scan approximately 8 MBq per kilogram of patient weight is required (Everaert et al, 2003). Local clinical experience has shown that on average, roughly 440 MBq of FDG is required at injection into the patient (Paul Cardew, Chief Nuclear Medicine Physics, John Hunter Hospital, Newcastle, NSW, Australia, Private

Communication). By dividing the fluorine-18 activity by 440 MBq, the number of patient doses of fluorine-18 can be calculated relative to the helium-3 irradiation time and the ability of the device for producing fluorine-18 for PET scans can be assessed assuming 50 % efficiency in synthesising fluorine-18 into FDG and mandatory Quality Control measurements.

5.4 Deuterated Mylar Target

For calculations of fluorine-18 yield from the deuterated solid target design an ion source emitting helium-3 at 1 MeV and at 100 mA was simulated on a pure Mylar target. The main effect of small target impurities would result in a small drop in the concentration of parent nuclei in equation 5 that would make a negligible difference in the yield calculation. It is noted that the beam corresponds to a 100 kW of power and that this will cause significant thermal effects in the target materials, however such a high power beam is chosen to produce clinically relevant activities of fluorine-18. The helium-3 ions were all assumed to be singly ionised and were targeted on a deuterated plastic target that had 100 % of all elemental hydrogen as the deuterium isotope. The helium-3 beam impinged the target over an area of 250 cm^2 giving a helium-3 current density on the target of 40 $\mu A/cm^2$. The thickness of the target was chosen to be 1 mm in an effort to find a balance between maximising the target lifetime due to material losses under ion bombardment and minimising the proton attenuation in the Mylar

5.4.1 Sputtering

Sputtering is a possible limiting factor in the Mylar target system as it determines the lifetime of the target. An estimate of the lifetime of the target due to sputter is made in the fluorine-18 yield calculations. Using the incident flux of Helium-3, determined from the measured beam the concentration of carbon in Mylar and the sputter coefficient for carbon from the Mylar target due to 1 MeV helium bombardment the rate at which the target is degraded can be calculated. As a measure of the target lifetime it was calculated using measured sputter coefficients

how much helium-3 beam time it took to sputter the target down to 0.5 mm (ie half the target thickness).

5.4.2 Proton Attenuation

Using SRIM simulations, the range of 1 MeV helium-3 in Mylar was calculated to be 3.59 μm. Such a range has a number of implications for the yield of the system. Firstly, although the thickness of the Mylar target is 1 mm the 3.59 μm range of the helium-3 in the Mylar means that only deuterium atoms in this range are available for reaction at any stage. This may appear to be a severe limitation on the system as it is reasonably expected that deuterium in this small range will quickly be used up. However, the sputter phenomenon now becomes advantageous as it constantly exposes new deuterium to the helium-3 for interaction.

The small range of the helium-3 in Mylar means that all protons produced via the $^{3}He(d,p)^{4}He$ reaction are produced towards the front surface of the Mylar target and then must traverse the majority of the Mylar to reach the heavy water and hence the oxygen-18. Significant proton attenuation can be expected along this journey. Once again sputtering becomes advantageous as it progressively shortens the distance the protons have to travel through the Mylar and hence minimises the amount of proton attenuation before reaching the heavy water. As the target decreases in thickness the efficiency of the system will improve in terms of yield. For a practical device the optimal thickness of the target must be found which balances yield efficiency with target lifetime.

Proton attenuation in the Mylar was accounted for in calculations by determining the proton energy loss in the Mylar and using the remaining energy as the initial proton energy for the total integrated cross section calculation for the $^{18}O(p,n)^{18}F$ reaction. The calculation of the proton energy-loss was performed similarly to the calculation in the total integrated cross section calculation where stopping powers were used to find the energy of the particle at incremental depths in the target material. Firstly, SRIM was used to calculate stopping powers for protons of energy up to 17.4 MeV in Mylar. With the initial average proton energy from the $^{3}He(d,p)^{4}He$ reaction of 16.6 MeV these stopping powers could be used to determine

the proton energy at each depth in the Mylar. The proton energy at 1 mm depth in the Mylar corresponds to the energy with which the proton emerges from the Mylar into the heavy water. This treatment does not account for the increase in proton energy emerging from the Mylar as the target sputters away and there is less proton attenuation, so in this regard the calculation is a worst-case-scenario. However, the effect in terms of fluorine-18 yield will be minimal due to the small reaction cross sections for the $^{18}O(p,n)^{18}F$ reaction above 10 MeV proton energy.

5.4.3 Helium-3 and Proton Losses

For the deuterated Mylar system the first possible losses due to competing nuclear reactions are between the helium-3 and the Mylar target. Such losses could include reactions between the helium-3 and carbon-12, helium-3 and oxygen-16 and reactions between helium-3 and deuterium other than the $^{3}He(d,p)^{4}He$ reaction. Investigation revealed no such reactions for helium-3 energies of 1 MeV and lower

The second stage of possible loss occurs while the protons traverse the Mylar before being exposed to the oxygen-18 in the heavy water target. In this stage the reactions of interest are those between protons and deuterium, protons and carbon-12 and protons and oxygen-16. Reactions of order mbarns or greater were adjudged significant as this was similar magnitude to the cross sections of the $^{18}O(p,n)^{18}F$ reaction. It was found that the reactions $^{16}O(p,\alpha)^{13}N$ and $^{12}C(p,p+2\alpha)^{4}He$ had cross sections of order mbarns in the energy range of 12 to 16 MeV, which is the energy range of the protons within the Mylar. While traversing the Mylar the protons are not in contact with oxygen-18 so any losses can simply be subtracted from the useable proton current available for the $^{18}O(p,n)^{18}F$ reaction. The amount of loss from the $^{16}O(p,\alpha)^{13}N$ and $^{12}C(p,p+2\alpha)^{4}He$ reactions was calculated using equation 5 and subtracted from the useable proton current for the $^{18}O(p,n)^{18}F$ reaction. This was achieved by utilising the proton energy with depth in the Mylar used in the calculation of proton attenuation in the Mylar. Cross sections for both the $^{16}O(p,\alpha)^{13}N$ and $^{12}C(p,p+2\alpha)^{4}He$ reactions were applied to each incremental depth based on the proton energy at that depth. Cross section data for these two reactions was obtained using the EXFOR database of the Nuclear Data Services section of the

IAEA Nuclear Data Centre. Values from Takacs, 2003 for the reaction cross sections of the $^{16}O(p,\alpha)^{13}N$ reaction in the energy range of 0 to 30 MeV were used and are presented in figure 18.

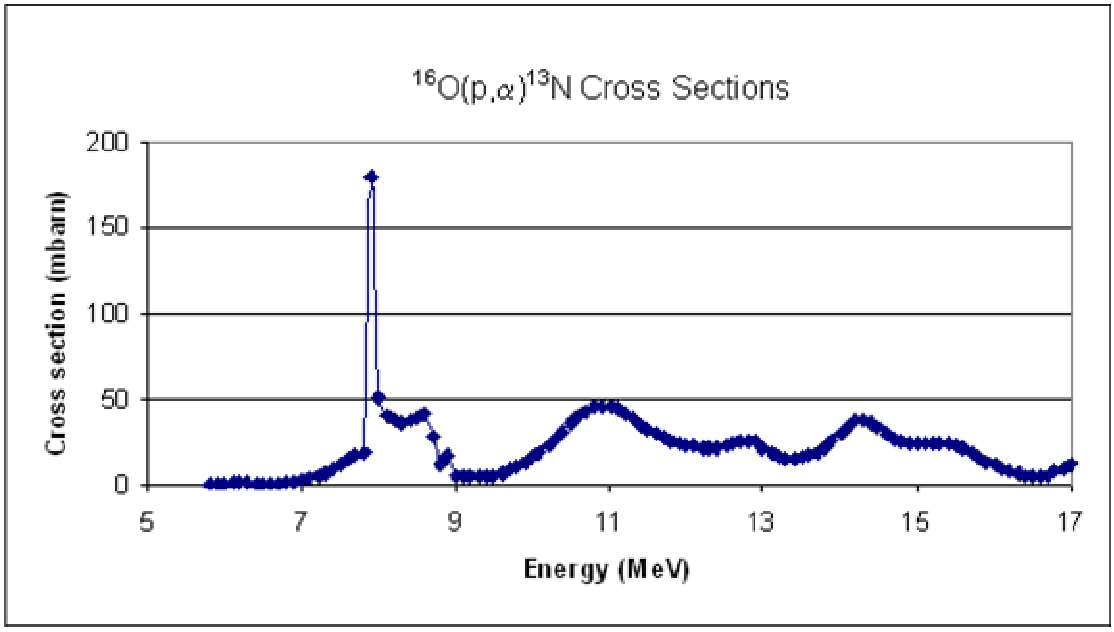

Fig 18 Reactions Cross Sections for the $^{16}O(p,\alpha)^{13}N$ reaction in the energy range 5 to 17 MeV. (Takacs et al, 2003).

By summing the cross sections assigned to the proton energy values with depth in Mylar and multiplying by the incremental depth the total integrated cross section used in equation 5 was obtained. The concentration of oxygen-16 in Mylar was then calculated and this was multiplied by the total integrated cross section and the proton current in the Mylar to determine how many $^{16}O(p,\alpha)^{13}N$ reactions occurred in the Mylar and hence how many protons were lost.

The process was repeated for the $^{12}C(p,p+2\alpha)^{4}He$ reaction. Data for the cross sections of the $^{12}C(p,p+2\alpha)^{4}He$ reaction was also found in the EXFOR database in the form of data presented by Harada et al, 1999 and MacLeod and Milne, 1972. Since the data only contains three data points between 13 and 18 MeV and no data points between 14 and 18 MeV a linear interpolation was made between 14 and 18 MeV to produce estimate data points at increments of 0.5 MeV. With this linear interpolation the data for the $^{12}C(p,p+2\alpha)^{4}He$ reaction is presented in figure 19.

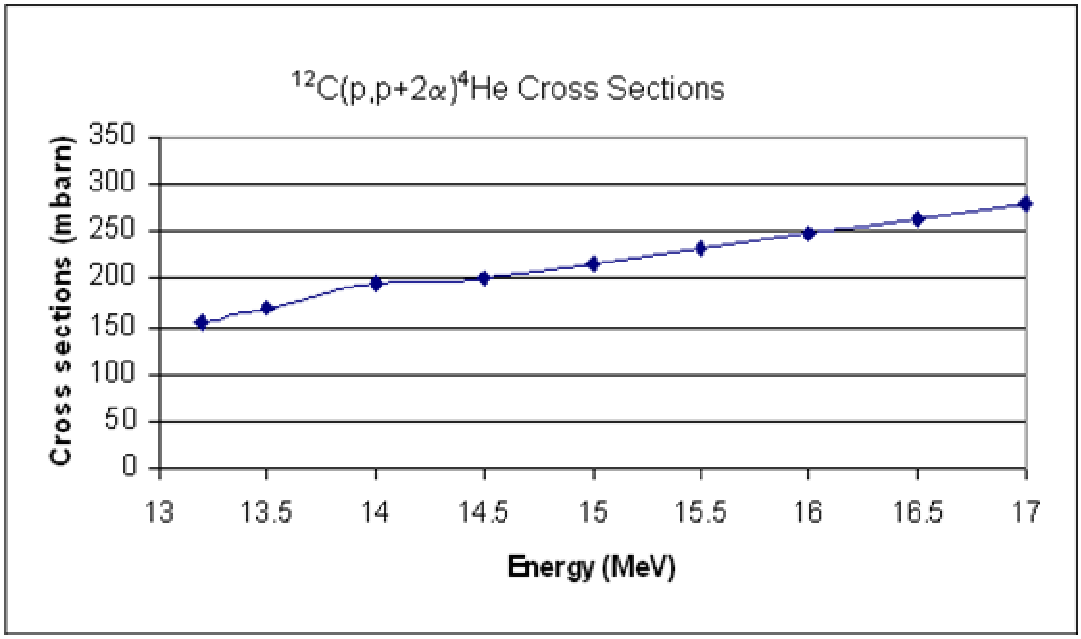

Fig 19 Reactions Cross Sections for the $^{12}C(p,p+2\alpha)^{4}He$ reaction in the energy range 13 to 17 MeV. (Harada et al, 1999, Macleod and Milne, 1972). Data interpolated between 13 and 18 MeV.

The third possible stage of proton loss occurs when the protons leave the Mylar and emerge into the oxygen-18 heavy water. At this stage reactions between the protons and hydrogen and reactions between the protons and oxygen-18 other than the $^{18}O(p,n)^{18}F$ reaction will be in competition with the $^{18}O(p,n)^{18}F$ reaction. The only possible significant reaction found was the $^{18}O(p,\alpha)^{15}N$ reaction. However, there are not enough cross section data available in the relevant energy range to predict the effect of this reaction of fluorine-18 yield. This is evident in figure 20.

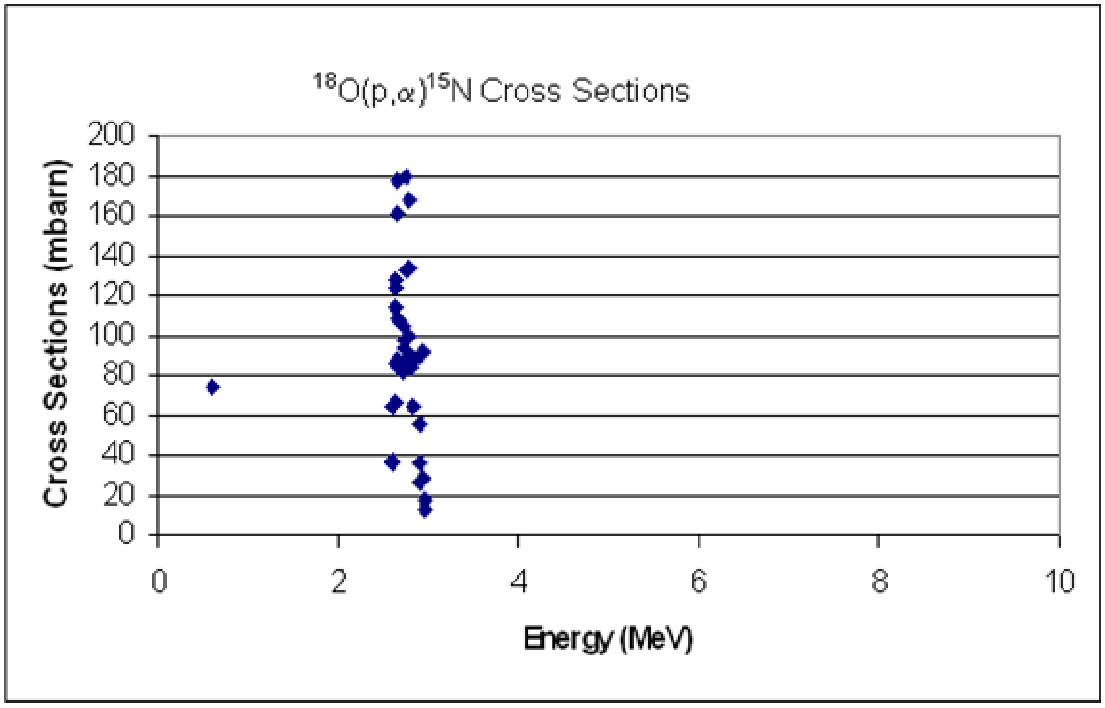

Fig 20 Available Reaction cross sections for the $^{18}O(p,\alpha)^{15}N$ reaction. Data from Blair and Leigh, 1960 and Amsel and Samual, 1967.

5.5 Super Heavy Water Target

As with the deuterated Mylar target design, calculations for the fluorine-18 yield of the super heavy water target design are made assuming a helium-3 ion source producing singly ionised 1 MeV helium-3 ions at a current of 100 mA. The target is assumed to be pure and the calculations are performed similarly to the deuterated Mylar system calculations using equation 5. To calculate the total integrated cross section for the $^{3}He(d,p)^{4}He$ reaction with the super heavy water system a SRIM simulation was performed of the 1000 keV helium-3 ions in super heavy water to calculate stopping power. From this simulation it was found that the 1 MeV helium-3 ion had a range of 5.08 μm in the super heavy water. This is approximately 1.5 times the range of the helium-3 ion in the Mylar and this combined with the increased deuterium concentration in super heavy water as compared with Mylar means that more deuterium is available for $^{3}He(d,p)^{4}He$ reaction in the super heavy water system compared with the deuterated Mylar system. This will make the super heavy water system relatively more efficient at

producing protons and should decrease the chance of deuterium being prematurely used up.

The constant sputtering of the target, which reveals new deuterium to the helium-3 ions means that the Deuterium is unlikely to be used up in the deuterated Mylar system and it has the same effect in the super heavy water system. The lifetime of the super heavy water target is less important than the lifetime of the Mylar target as the super heavy water does not have to support the vacuum. The super heavy water needs only to maintain enough thickness to cover the proton range in water so that the total integrated cross section of the $^{18}O(p,n)^{18}F$ reaction is always maximum. Unlike the Mylar target that has its thickness limited by the need to minimise the proton attenuation through the Mylar the super heavy water has no such limitation. The only limiting factor associated with the super heavy water thickness would be the cost of the super heavy water itself. In practice it is likely that the thickness of super heavy water would be chosen to be the minimum super heavy water required to produce the required fluorine-18.

One issue associated with sputtering of the super heavy water is in fluorine-18 recovery. As the fluorine-18 is essentially produced in the deuterium target for the helium-3 beam in the super heavy water system then it is certain that some of the fluorine-18 produced early in a run will be sputtered away. As this fluorine-18 cannot exit the vacuum system it is envisaged that a system of collecting all the sputtered material, most likely in liquid form and including sputtered fluorine-18, should be possible so that all the fluorine-18 can be extracted when the vacuum seal is broken. However, sputtered super heavy water also poses the problem of interacting with the helium-3 beam and this is another consideration that must be resolved with any practical system.

5.5.1 Helium-3 and Proton Losses

Possible losses in the super heavy water system are two staged and can be either helium-3 loss or proton loss. Besides the reactions already mentioned in the deuterated Mylar system section, the helium-3 can also come into contact with

hydrogen in the super heavy water system, but no significant reactions between helium-3 and hydrogen were found below 1 MeV.

Once the $^{3}He(d,p)^{4}He$ reaction has taken place the product protons are able to react with deuterium and oxygen-18. Besides the $^{18}O(p,n)^{18}F$ reaction used to produce fluorine-18, three other significant reactions occur for proton energy below 17 MeV. These include $D(p,\gamma)^{3}He$, D(p, n+p)H and $^{18}O(p,\alpha)^{15}N$. Similarly to the deuterated Mylar system calculations, the effect of the $^{18}O(p,\alpha)^{15}N$ reaction could not be investigated due to lack of cross section data although from the limited data available it could be surmised that this reaction could be significant. This also applied to the D(p, n+p)H reaction of which the available cross section data provided by Gibbons and Macklin, 1959 is presented in figure 21.

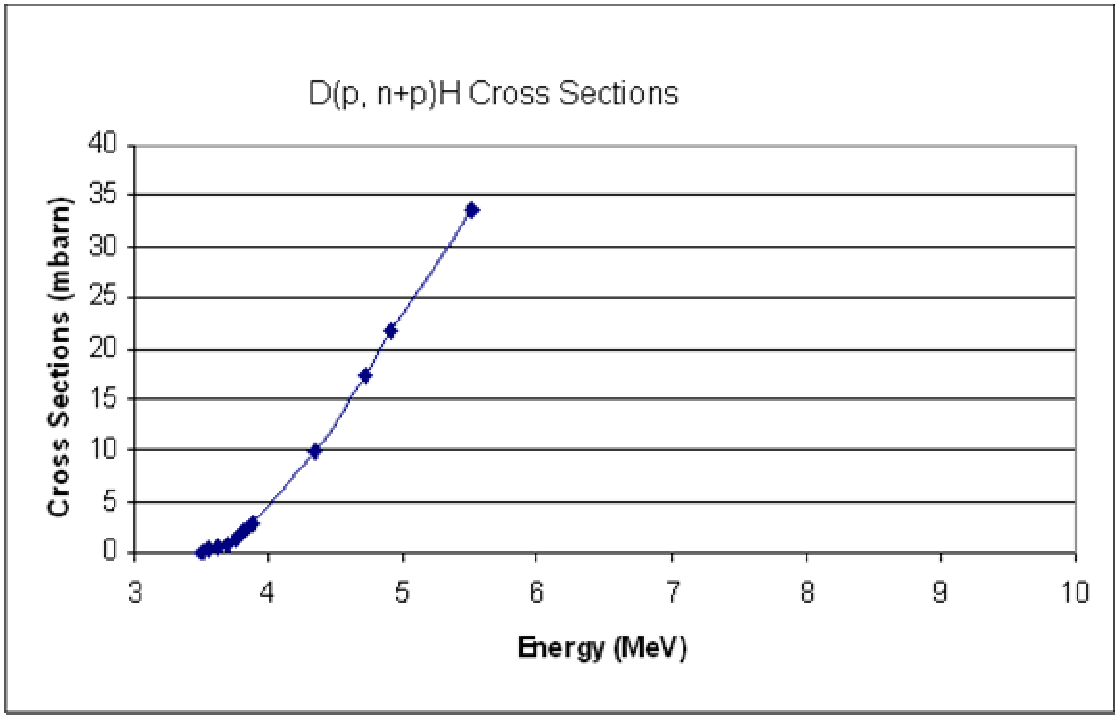

Fig 21 Reaction Cross Sections for the D(p, n+p)H reaction. Gibbons and Macklin, 1959.

As with the deuterated Mylar calculations the yield from the $D(p,\gamma)^{3}He$ reaction was calculated using equation 5. Because this reaction occurs concurrently with the $^{18}O(p,n)^{18}F$ reaction it is difficult to calculate the precise yield as the

occurrence of a reaction will obviously prevent the proton being available for another reaction. This combined with the different energy dependence of cross section for each reaction makes precise calculations of yields difficult. As such, yields from each reaction were compared independent of each other and the magnitude of yields compared to attain a qualitative measure as to the significance of the $D(p,\gamma)^3He$ reaction on fluorine-18 yield. The cross sections data used for the $D(p,\gamma)^3He$ reaction are provided by Matthews et al, 1974, Skopik et al, 1979, Griffiths, 1962.

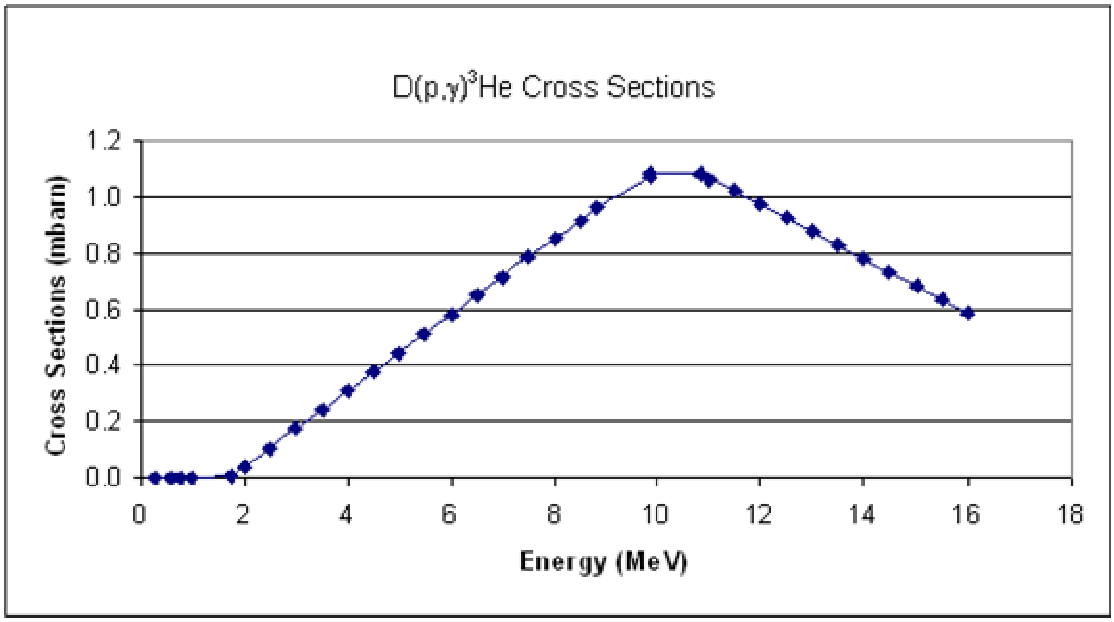

Fig 22 Reaction Cross sections for the D(p,γ)He3 reaction as provided by Matthews et al, 1974, Skopik et al, 1979, Griffiths, 1962. Linear interpolation of cross sections was performed between 1.75 MeV and 8.83 MeV and between 10.83 MeV and 16 MeV.

The calculations presented express a means of estimating fluorine-18 yield from two different system designs. They require as inputs the initial helium-3 beam current and energy. These values have been chosen to optimise yield while still being feasible for known saddle-field ion sources. Factors such as sputtering, attenuation and particle loss either due to particles exiting the system or being consumed in competing nuclear reactions are all investigated. The final yield taking into account such losses provides an indication as to whether either the deuterated

Mylar target system or the super heavy water system should be investigated experimentally as an alternate method of producing fluorine-18 for PET applications.

The method of calculating fluorine-18 yield has now been outlined. The two system designs provide the calculation geometry required to apply the calculation method and the initial beam parameters of 100 mA and 1 MeV for the helium-3 beam have been chosen to produce clinically useful yields of fluorine-18 despite the problems of sputtering and thermal effects in the target due to the 100 kW beam. As such, it is now possible to calculate the yield of fluorine-18 from the deuterated Mylar system and the super heavy water system.

6. Results and Discussion

In the following chapter the results for the fluorine-18 yield calculations will be discussed. Firstly, the deuterated target design will be assessed in terms of its fluorine-18 yield and then its performance and limitations evaluated. The alternative super heavy water design will be similarly analysed and the two competing systems are compared and contrasted for relative strengths and weaknesses. Finally, issues that apply to both designs are addressed.

6.1 Deuterated Target

The yield of fluorine-18 with beam-on time for the Mylar-target system is shown in figure 23, calculated using the methods outlined in Chapter 5. The parameters used in calculation of the yields were:

Input beam – 1 MeV singly ionised He-3 at 100 mA over 250 cm^2

Target – 1 mm thick deuterated Mylar

Medium – H_2O^{18} on the opposite side of the Mylar target to the ^3He beam

The calculations account for decay of fluorine-18 during the irradiation process. In Figure 23, fluorine-18 yields are shown both in total accumulated activity (left axis) as well as number of patient doses (right axis, based on an estimate of 440 MBq per patient dose). Calculations were performed at 0.5 hr resolution.

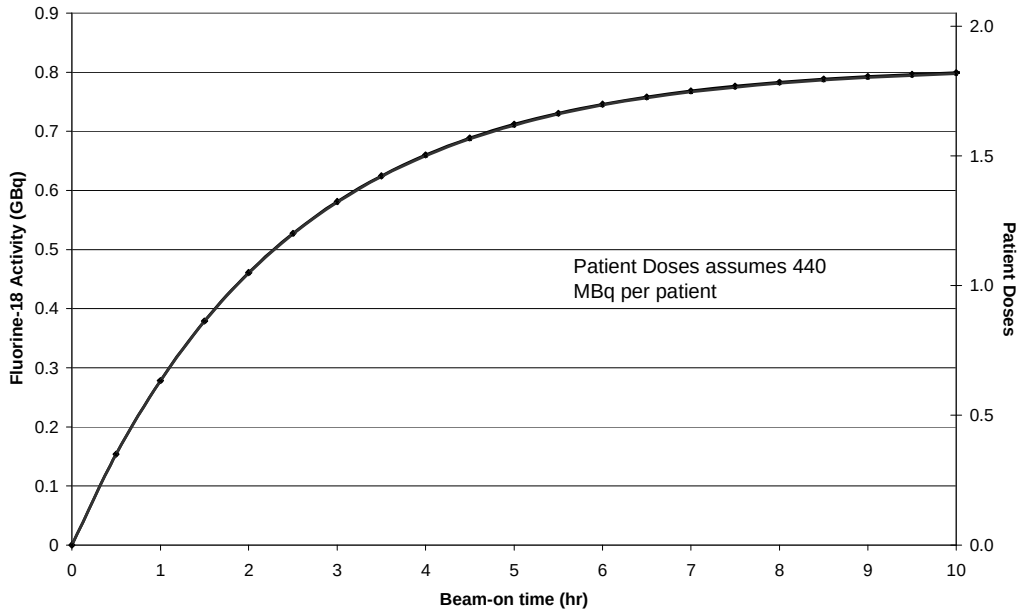

Fig 23 Yield of fluorine-18 produced with varying helium-3 beam on time for the Deuterated Mylar system.

The results reveal that, ignoring practical issues, the Mylar system would be capable of producing enough fluorine-18 for single patients with a helium-3 ion source operating at 1 MeV and 100 mA. A positive feature of the Mylar design is that different amounts of fluorine-18 activity can be produced as required by altering the time the beam is on. This is made possible by the fact that the heavy water in which the fluorine-18 is in solution is not under vacuum and hence extraction of the fluorine-18 can be performed without breaking the vacuum. This would allow more flexible operation and allow multiple individual batches of fluorine-18 to be made in a single day, which would be impossible if the vacuum had to be broken for fluorine-18 extraction. It is envisaged that production of fluorine-18 would be made immediately prior to the scan such that each patient's fluorine-18 could be made individually. In practice such a procedure would involve producing the fluorine-18 for the next patient while the former patient is being scanned. The image acquisition time for current PET of 15 to 25 minutes is already a constraint on the number of patient scans possible per day and hence provides some time for fluorine-18 production. The great advantage of producing fluorine-18 doses individually is that it minimises loss due to decay before being injected into the patient.

The simulations show that when the ion beam is on for one hour approximately 278 MBq of fluorine-18 is produced and that if the beam on time is 2 hours the yield increases to approximately 461 MBq (figure 23). Based on the generalism that 8 MBq is required per kilogram of patient mass to guarantee a high quality scan (Everaert et al, 2003) then the 2 hour beam time produces enough fluorine-18 for a whole body PET scan of a patient of 58 kg. Increasing the beam on time will further increase the fluorine-18 yield and hence the system would be capable of producing enough fluorine-18 to PET scan any patient requiring the procedure. For a typical patient of say 70 kg, 560 MBq of fluorine-18 is required and could be produced with 3 hours beam on time, which would allow for a loss of 50 % of activity in the fluorine-18 recovery from the heavy water or FDG synthesis process. Three hours beam on time per patient, which would be longer for patients above 70 kg, would severely limit the number of patients scanned per day and hence make the system unfeasible

6.1.1 Replacing Mylar with Plexiglas

From the information provided in table 3 Plexiglas is shown to have 1.82 times the concentration of deuterium than Mylar. Based on this, Plexiglas was used to replace Mylar in the fluorine-18 yield calculations and the results are presented in figure 24.

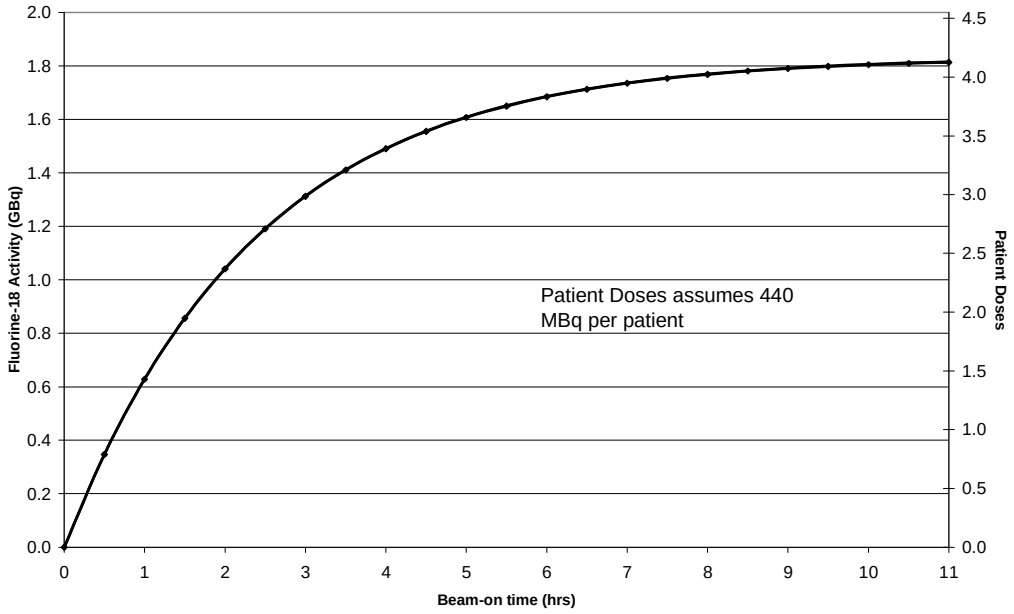

Fig 24 Yield of fluorine-18 produced with varying helium-3 beam on time for the Deuterated Plexiglas system.

Figure 24 shows a significant increase in yield of fluorine-18 by replacing the deuterated Mylar target with a deuterated Plexiglas target. For the Plexiglas system, one hour beam on time with 1 MeV helium-3 at 100 mA produces 629 MBq of fluorine-18, which is enough to perform a whole body scan of a patient weighing 79 kg allowing for 50 % loss of fluorine-18 in the processes prior to injection into the patient and this is approximately twice the yield using the Mylar target. This outcome is predominantly due to the increase in deuterium concentration, but the lower stopping power of helium-3 in Plexiglas than in Mylar due to the lower relative concentrations of carbon and oxygen also plays a role. Hence, 1 MeV helium-3 has a longer range in Plexiglas (5.02 μm) than in Mylar (4.3 μm) and subsequently has greater chance of interacting with the deuterium via the $^{3}He(d,p)^{4}He$ reaction. It should be noted that the performance of Plexiglas in vacuum and under ion bombardment is not as well understood as for Mylar and this could lead to decreased performance under practical conditions. The well known characteristics of Mylar were a main reason why it was chosen as the primary deuterated plastic investigated in this study.

6.1.2 Target Degradation

Having established an optimum condition and material for this process, it is essential that the practicality of these be evaluated. Under 1 MeV helium-3 bombardment degradation of the plastic target can be expected. Such degradation includes loss of target due to target atoms being sputtered, blistering of the target surface (Shrinet et al, 1986) and changes in the structure of the surface of the polymer due to cleavage of chemical bonds along the ion trajectory. (Hnatowicz et al, 2000). The two main sources of target degradation are expected to be sputtering and heating due to energy transfer from the helium-3 beam. For a 1 MeV helium-3 beam at 100 mA, 100 kW of power is transferred to the target. As the plastics are poor conductors of heat, the worst case scenario of heat dissipation by radiation will be considered. The equilibrium temperature that the target will reach can be determined using the Stefan-Boltzmann law.

$$P = \varepsilon \sigma A T^4 \qquad (6)$$

where: ε = total emissivity of the target
σ = universal gas constant = 5.67×10^{-8} W/m^2.K^4
A = Area of radiating surface
T = absolute temperature in Kelvin

Using the parameters of the system design it was estimated that due to helium-3 bombardment the Mylar target would be heated to approximately 2570 °C. The emissivity of Kapton at 0.94 was used as an estimate for the emissivity of Mylar. The melting point of Mylar is approximately 250°C (http://www.grafixplastics.com), which is much lower than the predicted equilibrium temperature of 2570 °C. Therefore, heat effects due to the ion implantation will be prohibitive. Some possible methods of mitigating this 2570 °C temperature rise could be to increase the target surface area under bombardment from the currently used value of 250 cm^2 and employing a target cooling system, possibly liquid nitrogen, in an attempt to help dissipate the heat. Such remedies would be unlikely to keep the target below its melting point.

Sputtering is a significant issue in that sputtered target atoms will deplete the target affecting its ability to act as barrier to hold vacuum. Also, sputtering of deuterium could potentially lead to a decrease in deuterium available in the target for the $^{3}He(d,p)^{4}He$ reaction leading to a drop in the proton beam current and hence yield of fluorine-18. A calculation was performed using the incident helium-3 current and sputter coefficient of helium-3 in polymer targets to determine the target lifetime. For the Mylar target system and a helium-3 beam of 1 MeV and current density of 0.4 mA/cm^2 associated with the 250 cm^2 target irradiation area, the sputter rate was found to be 4.27 μm/hour. This assumed a sputter coefficient of 2.0 atoms/ion. This sputter coefficient was estimated from the work of Rovner and Chen (1974) in the absence of any better data. This means that for a 1 mm thick target the beam time for half the target to be sputtered is approximately 117 hours. In practice, this target lifetime is quite short and changing the target so often would likely be a burden on a clinical department. Using 117 hours target lifetime, the total amount of fluorine-18 that can be produced in a target's lifetime can be calculated for varying lengths of fluorine-18 production runs and is presented in figure 25.

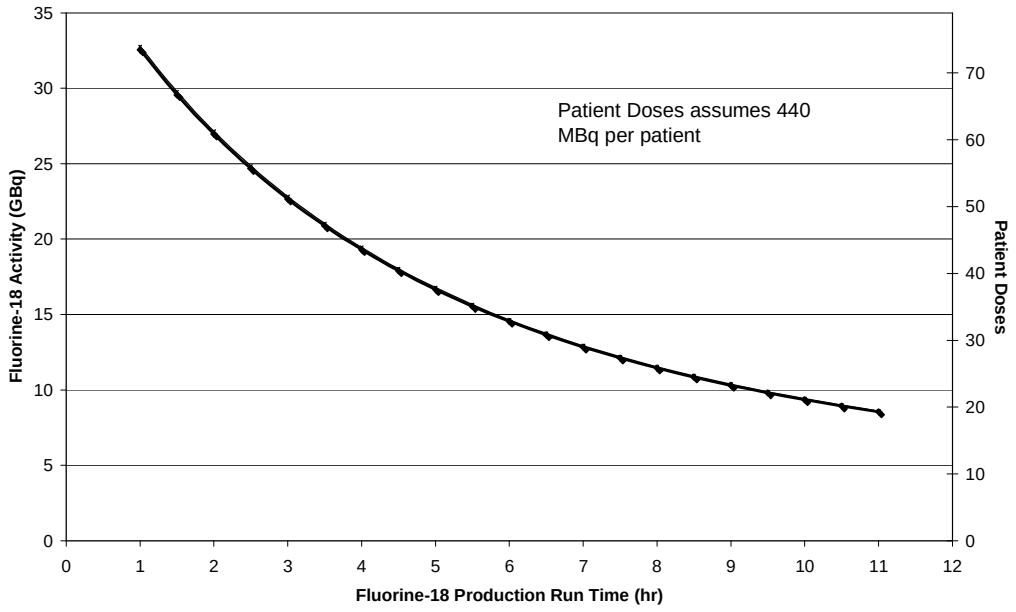

Fig 25 Yield of fluorine-18 for a single target with varying fluorine-18 Production run times highlighting how much total fluorine-18 can be produced before a target needs to be changed

If the system is used as envisaged with beam on times of approximately one hour then almost 33 GBq of fluorine-18 can be produced per Mylar target. Results are not presented for fluorine-18 production runs less than one hour because for less than one hour not enough fluorine-18 is produced to scan an average sized patient. The results show that short production run times are most effective for maximising the fluorine-18 yield per target. This is because the loss of fluorine-18 due to decay during the production process is minimised. Maximising the fluorine-18 yield per target is important for ensuring that the system is economically feasible. There is also an important practical advantage in that to change the target it is necessary to spoil at least part of the vacuum. As such replacing a target is both time consuming and requires technical expertise and thus minimising the number of required target changes is important.

6.1.3 Effect of Unwanted Nuclear Reactions in the Deuterated Target system

For the deuterated target system only two unwanted nuclear reactions were found that would take place and have any significant impact on the yield of fluorine-18. These two reactions are $^{16}O(p,\alpha)^{13}N$ and $^{12}C(p,p+2\alpha)^{4}He$. The two reactions work to minimise the number of protons available to react with oxygen-18 to form fluorine-18. It should be noted that in the case of the $^{12}C(p,p+2\alpha)^{4}He$ reaction the total number of protons available for reaction with oxygen-18 is the same before and after reaction with carbon-12. The result of the reaction however would be a significant decrease in the proton energy between the proton initiating the reaction and the one produced by the reaction due to energy being distributed to the product alpha particles. Since the cross section of the $^{18}O(p,n)^{18}F$ reaction drops sharply below 5 MeV and the threshold energy for the reaction is about 2.5 MeV (figure 8) then such a drop in proton energy would decrease the yield of fluorine-18.

From calculations of the number of $^{16}O(p,\alpha)^{13}N$ and $^{12}C(p,p+2\alpha)^{4}He$ for the deuterated target system using equation 5 it is estimated that about 1.28×10^{8} protons/s would be lost to these reactions. The system is expected to generate 1.85×10^{12} protons/s. As such, these alternative reactions will lead to the loss of less then 1

in 10 000 protons. Although insignificant, this loss has been taken into account in the available proton current for the $^{18}O(p,n)^{18}F$ reaction.

6.2 Super Heavy Water Target

Due to the limitations of the deuterated target design an alternative design based upon a single super heavy water target was also investigated. Such a design had expected advantages over the deuterated target design in terms of target degradation and efficiency.

With a helium-3 ion source producing 1 MeV singly ionised helium-3 ions at a beam current of 100 mA targeted onto super heavy water (D_2O^{18}), the yield of fluorine-18 produced is shown in figure 26.

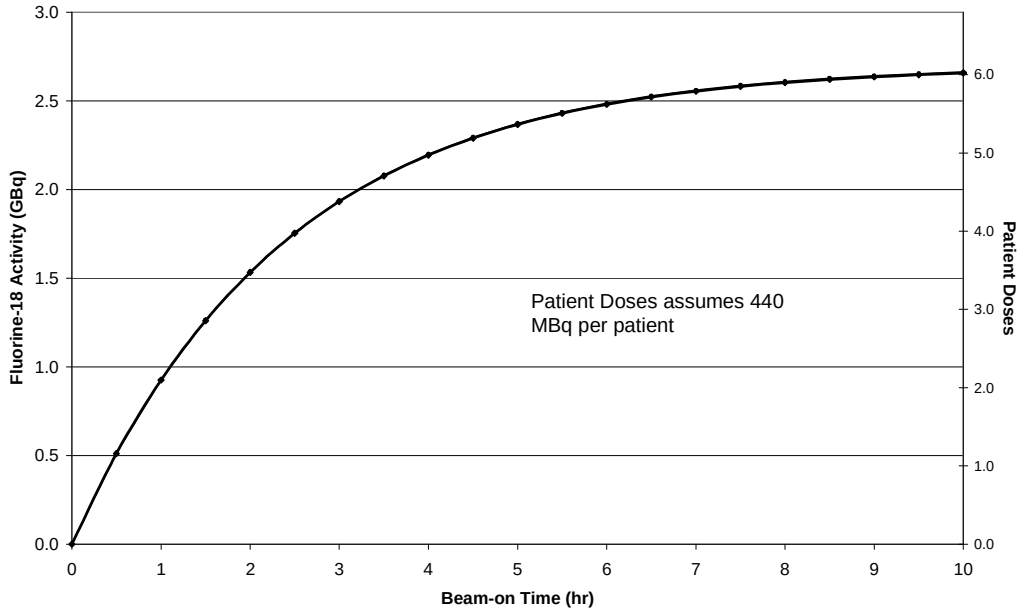

Fig 26 Yield of fluorine-18 produced with varying helium-3 beam on time for the super heavy water system.

The results show that for a 1 MeV, 100 mA helium-3 beam, the super heavy water system provides greater yield of fluorine-18 than the deuterated Mylar/Plexiglas target system. For a one hour production run time, 925 MBq of fluorine-18 is produced, which is enough for three scans of patients of 70 kg with a 50% loss margin. This is approximately 50% more yield then for the corresponding

production run time for the Plexiglas system and approximately 200 % more yield than from the Mylar system.

One reason for greater yield from the super heavy water system than the deuterated plastic target system is that there is minimal proton energy loss in traversing a deuterated target before coming into contact with the oxygen-18. Also, the concentration of deuterium in super heavy water is approximately 10 % greater than in deuterated Plexiglas and almost 100 % greater than in deuterated Mylar. This fact along with the decrease in stopping power of helium-3 in super heavy water compared to Mylar or Plexiglas because of the absence of carbon leads to higher efficiency in proton production via the $^{3}He(d,p)^{4}He$ reaction. This is borne out in the proton current produced in the super heavy water system compared to the deuterated plastic target systems with proton current of 0.69 μA produced in the super heavy water system and 0.63 μA and 0.30 μA produced in the deuterated Plexiglas and Mylar systems respectively.

A disadvantage of the super heavy water system to the deuterated plastic target systems is that the oxygen-18 and hence the product fluorine-18 is under vacuum. This makes extraction of the fluorine-18 a much more involved process. Because of this it is more likely that with the super heavy water system, one long fluorine-18 production run would be used to produce multiple patient doses. An example can illustrate this point; Common work practice would involve the super heavy water system being used to produce fluorine-18 immediately prior to the first scan of the day. If four patients required PET scans in a single day with an image acquisition time of one hour, the super heavy water system would have to have five hours production run time to produce enough fluorine-18 to inject each patient with 440 MBq of FDG (taking into account decay of fluorine-18 throughout the day). This allows for 50 % loss of fluorine-18 during extraction and FDG synthesis.. Being able to only scan four patients a day and requiring a five hour fluorine-18 production run is unfeasible for a clinical department.

6.2.1 Target Degradation

The issue of sputtering, while more pertinent to the deuterated Mylar system is still relevant to the super heavy water system. Sputtering is both detrimental and advantageous to fluorine-18 production. Sputtering is advantageous in that it constantly exposes new deuterium to the helium-3 beam which is important considering the relatively short range of helium-3 in water. Sputtering also determines the required thickness of super heavy water. Sputter coefficients for helium atoms with energy as high as 1 MeV could not be found. However, the work of Baragiola et al, 2003 and Fama et al, 2008 for helium atoms of 100 keV and lower found sputter coefficients for helium atoms on water ice of the order of 10 ions/atom. It is unlikely that such a sputter coefficient would apply for MeV helium atoms, but if it did then it is calculated that approximately 0.7 mm of target would be sputtered away for every hour of beam time. Depending on the number of patient doses of fluorine-18 required and hence the required beam time this could be used to calculate the minimum required super heavy water target thickness.

Sputtering also has a detrimental effect in fluorine-18 production. Sputtered particles will potentially degrade the vacuum required for the helium-3 beam and also spread the product fluorine-18 around the vacuum chamber making it more difficult to extract.

To utilise super heavy water as a target it needs to be in solid form. This can easily be achieved using liquid nitrogen but means that heat effects due to ion implantation can be a significant issue. For the 1 MeV helium-3 beam at 100 mA target onto an area of 10 cm^2 as was used for fluorine-18 yield calculations, the temperature of the super heavy water would rise by approximately 6174 °C. Such a large temperature rise would rapidly vaporize the target and it is highly unlikely if this could be prevented in a feasible system by remedies such as increased target area or by a cooling system.

6.2.2 Effect of Unwanted Nuclear Reactions in the Super-Heavy-Water System

Three unwanted nuclear reactions were found to occur in the super heavy water system that could impact on the yield of fluorine-18. Similarly to the deuterated target system, no helium-3 reactions were identified. However, there are proton reactions including $D(p,\gamma)^3He$, D(p,n+p)H and $^{18}O(p,\alpha)^{15}N$. As these reactions are all proton reactions and are occurring in the presence of the oxygen-18 then they are in direct competition with the $^{18}O(p,n)^{18}F$ reaction. As such, the yields from these reactions cannot simply be subtracted from the available proton current for the $^{18}O(p,n)^{18}F$ reaction and it is difficult to quantify the effects of these reactions on the fluorine-18 yield. By performing yield calculations using equation 5 for the above-mentioned reactions in isolation of each other a rough estimate of yields can be calculated. The yield of the $D(p,\gamma)^3He$ reaction is estimated to be 1 % of that of the $^{18}O(p,n)^{18}F$ reaction and as such is relatively insignificant. An indirect benefit of this reaction is that it would increase the helium-3 beam current slightly but this is offset in that the effect of the reaction is also to minimise the available deuterium concentration.

The yield of the D(p,n+p)H reaction is estimated to be approximately 2 % of that of the $^{18}O(p,n)^{18}F$ reaction which again is relatively insignificant. The products of this reaction result in an increase in available proton current. However, as with the $^{12}C(p,p+2\alpha)^4He$ in the deuterated target system the protons produced from the D(p,n+p)H reaction would have significantly less energy than the initial proton. As neutrons and protons have roughly the same mass it follows that the energy from the D(p,n+p)H reaction would be distributed fairly evenly between the three product particles. With initial average proton energy of approximately 17 MeV, the product protons would each have a maximum of about 5.5 MeV and the majority would have far less than this. Because of the rapid decline in reaction cross section below 5 MeV for the $^{18}O(p,n)^{18}F$ reaction demonstrated in figure 8 then the contribution of protons from the D(p,n+p)H reaction towards producing fluorine-18 would be minimal.

The estimated yield from the $^{18}O(p,\alpha)^{15}N$ reaction is calculated to be approximately 2.2 % of the yield from the $^{18}O(p,n)^{18}F$ reaction which again is relatively insignificant. The $^{18}O(p,\alpha)^{15}N$ reaction works to minimise the amount of oxygen-18 available for the $^{18}O(p,n)^{18}F$ reaction, but countering this is the fact that fluorine-18 decays back to oxygen-18, such that any fluorine-18 that decays before irradiation is finished will revert back to oxygen-18 that can be converted back to fluorine-18 again. Interestingly the $^{16}O(p,\alpha)^{13}N$ reaction listed as a cause of proton loss in the deuterated target system produces nitrogen-13 which is one of the PET isotopes listed in table 1. It could be speculated that using standard D_2O^{16} heavy water as the target in the super heavy water design then nitrogen-13 could be produced as a PET isotope. However, the small reaction cross sections of the $^{16}O(p,\alpha)^{13}N$ reaction, typically in the order of 10 mbarns in the relevant energy range, coupled with the short half life of nitrogen-13 of 9.9 minutes would make such a proposition unfeasible.

6.3 Issues common to both the Deuterated target and Super Heavy Water Designs

6.3.1 Radiation Protection

A major detriment to using methods involving the $^{18}O(p,n)^{18}F$ reaction for fluorine-18 production concerns radiation protection. In the $^{18}O(p,n)^{18}F$ reaction used to produce fluorine-18 an energetic neutron is produced for every fluorine-18 atom produced. Neutrons pose a significant radiation protection threat due to their high penetration and tendency to activate nuclei with which they come into contact. As a result a variety of unstable nuclei are formed with varying half-lives in places beyond typical X-ray shielding. This can cause an increased radiation background long after the system has stopped operation. To attain a measure as to how much of a radiation hazard our device would cause, a calculation was performed to determine the neutron energy from the $^{18}O(p,n)^{18}F$ reaction. This calculation was performed similarly to the proton energy calculation in section 5.3.4. The results of this calculation are presented in Figure 27.

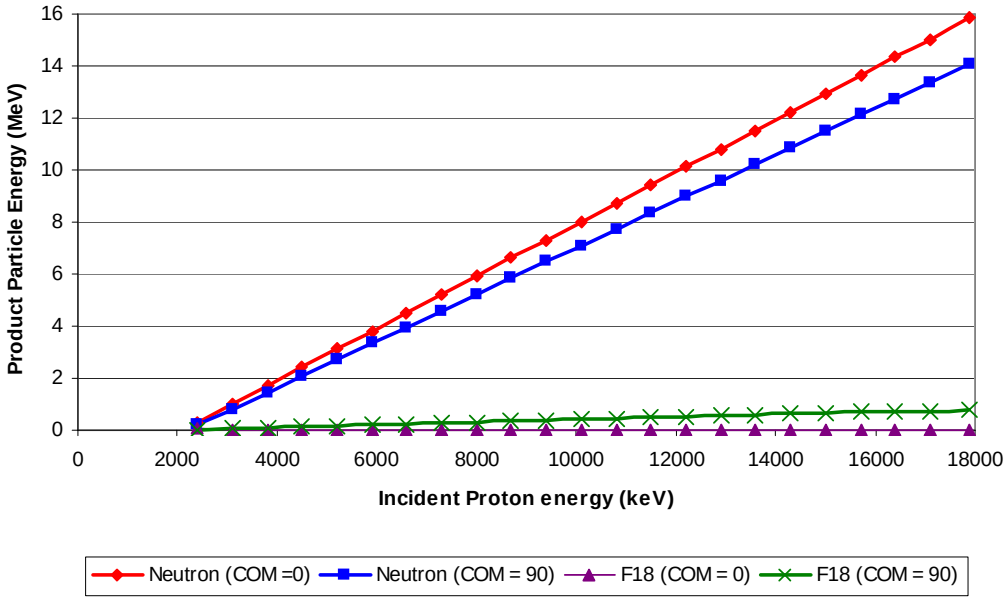

Fig 27 Calculated neutron and fluorine-18 energies for both 0 and 90 degrees emission angle in the COM frame from the $^{18}O(p,n)^{18}F$ reaction. Product particle energy is plotted against input proton energy.

Results show that neutrons are produced in the $^{18}O(p,n)^{18}F$ reaction with energy ranging from about 16 MeV down to thermal energies. Aside from the direct hazards of neutron production, the super heavy water system poses a radiation hazard due to the production of tritium from the neutrons interacting with deuterium. Tritium is an unstable isotope of hydrogen that decays via beta emission. The feature that causes tritium to be dangerous is it's relatively long half life of approximately 12.3 years (Krane, 1988) and the fact that it is a hydrogen analogue and so integrates easily into DNA. However, its removal from water is a relatively common procedure.

6.3.2 Shielding

The $^{18}O(p,n)^{18}F$ reaction is known to create a broad spectrum of neutrons as indicated in figure 27. Such neutrons as well as prompt gammas and gammas produced from neutron capture in the system pose a significant radiation safety hazard. Medical cyclotrons also use the $^{18}O(p,n)^{18}F$ to produce fluorine-18 so would pose a similar hazard. Such cyclotrons are sometimes located in specially shielded rooms but some designs incorporate self shielding. Such self shielding would likely

also be appropriate for the systems presented here. One example of a self shielded cyclotron is the CTI RDS system (Computer Technology and Imaging Inc, Berkeley, CA.). This system is surrounded by six interlocking shielding blocks on hydraulic tracks. Each block is composed of 0.2 m thick lead blocks which surround the targets and are used to attenuate any gamma rays produced. The lead blocks are then followed by 0.8 m of a mixture of Portland cement, boron carbide and polyethylene which is used to moderate and absorb neutrons (Hertel et al, 2004). The need for such shielding would significantly influence the practicality of the system in that it would significantly increase costs and require a relatively large, dedicated space for the system making it difficult to transport easily.

In 2004, Hertel et al performed a radiation survey of their CTI RDS self shielded cyclotron using Bonner sphere spectrometry. Hertel et al, found the neutron dose equivalent from the cyclotron immediately outside the shielding ranged between 9.3 and 0.28 mSv/y and the gamma dose ranged between 16 and 9.7 mSv/y. This was based on the assumption that the cyclotron produced 61 GBq of fluorine-18 per production run and that five runs were made per week over the year. They also assumed that the cyclotron room had zero occupancy during a production run. The dose readings they measured were well below occupational dose limits (Hertel et al, 2004).

The results show that both the deuterated target and super heavy water systems can produce relevant amounts of fluorine-18. However, both systems have significant practical issues revolving around sputtering and target degradation, target heating, radiation safety and the production of unwanted by products. Practical solutions do exist that could help to minimise the effects of a number of these issues and they can be further minimised through work practices that optimise fluorine-18 production run times to preserve the target and maximise efficiency, however such remedies will likely be insignificant and not result in the systems being feasible.

7. Conclusions

From a purely theoretical perspective, both the deuterated target and the super heavy water systems have been shown to be able, with a 100 mA, 1 MeV helium-3 beam, to produce an amount of fluorine-18 that could be used for a single PET scan. The beam parameters are at the extreme limit of saddle field ion source capability and still the amount of FDG produced would not be sufficient to supply the daily requirements of FDG for a PET centre scanning multiple patients daily. The issue of excessive target heating is a major practical difficulty. The equilibrium temperatures, calculated in the thousands of degrees Celsius, would quickly vaporize the targets making them unusable. It is unlikely that a solution could be found to remedy this problem.

The main issue for producing fluorine-18 revolves around the inefficiency of using a two step nuclear reaction process. Both the $^{3}He(d,p)^{4}He$ and $^{18}O(p,n)^{18}F$ steps in the process are quite inefficient and this means that a high current, high energy Helium-3 beam is required to produce significant fluorine-18. The high Helium-3 beam energy and current not only pushes Saddle-field ion source to the limit of its capability but also results in prohibitive target heating.

Radiation safety issues are also significant with both systems. The energetic neutrons produced by the $^{18}O(p,n)^{18}F$ reaction would require significant shielding to either system that would greatly increase the cost and limit mobility. The super heavy water system has the additional radiation safety problem of tritium production. Although extraction of tritium from water is a well established process, it adds another required step in the process and a possible extra source of fluorine-18 loss.

The effect of unwanted nuclear reactions occurring in either system appears to have minimal effect on fluorine-18 yield. However, the by products of such reactions would need to be studied to ensure the safety of either system.

Of the two designs investigated, the super heavy water system has been demonstrated to have greater fluorine-18 production efficiency, but it is likely that the deuterated plastic system has greater prospect for solving the practical issues. Neither system is considered to be viable in a clinical department

8. References

Amsel, G. & Samual, D. Microanalysis of the Stable Isotopes of Oxygen by Means of Nuclear Reactions. *J. Anal. Chem. 1967; 39; p 1689.*

Bailey, D. L., Townsend, D. W., Valk, P. E., & Maisey, M. N. (Eds). (2004). Positron Emission Tomography. Basic Sciences. Springer-Verlag. Singapore.

Bair, J. K. Total Neutron Yields from the Proton Bombardment of 17,18O. *Phys. Rev. C. 1973; 8(1); p120-123.*

Baragiola, R. A., Vidal, R. A., Svendsen, W., Schou, J., Shi, M., Bahr, D. A. & Ateberrry, C. L. Sputtering of Water Ice. *Nucl. Instr. Meth B. 2003; 209; pp294-303.*

Bishop, A., Satyamurthy, N., Bida, G., Phelps, M., & Barrio J. R. Production of [^{18}F]F_2 Using the ^{16}O(^{3}He,p)^{18}F Reaction. *Nucl. Med. Biol. 1996; 23; p 385-389.*

Blair, J. M., &Leigh, J. J. Total Cross Sections of the O18(p,α)N15 and O18(p,n)F18 Reactions. *Phys. Rev. 1960; 118(2); p 495-498.*

Blessing, G., Coenen, H. H., Franken, K., & Qaim, S. M. Production of [^{18}F]F_2,H^{18}F and $^{18}F_{aq}$ Using the Ne20(d,α)F18 Process. *Appl. Radiat. Isot. 1986; 37; p 1135.*

Bonner, T. W., Conner, J. P., & Lillie, A. B. Cross Section and Angular Distribution of the He3(d,p)He4 Nuclear Reaction. *Physical Review. 1952; 88(3); p473-476.*

Casella, V., Ido, T., Wolf, A. P., Fowler, J. S., MacGregor, R. R., & Ruth, T. J. Anhydrous F-18 Labeled , Elemental Fluorine for Radiopharmaceutical Preparation. *J. Nucl. Med 1980; 21; p 750*

Everaert, H., Vanhove, C., Lahoutte, T., Muylle, K., Caveliers, V., Bossuyt, A., & Franken, P. optimal dose of 18F-FDG required for whole-body PET using an LSO PET camera. *Eur. J. Nucl. Med. Mol. Imaging. 2003; 30(12); p1615-1619.*

Erasmus, J. J. & Sabloff, B. S. CT, Positron Emission Tomography and MRI In Satging Lung Cancer. *Clin. Chest Med. 2008; 29; p39-57.*

Fama, M., Shi, J. & Baragiola, R. A. Sputtering of Ice by Low Energy Ions. *Surface Science 2008; 602; pp156-161.*

Fawdry, R. M. A Simple Effective Method for Estimating the [^{18}O] Enrichment of Water Mixtures. *Appl Radiat. Isot. 2004; 60; p 23-26.*

Franks, J. Properties and Applications of Saddle-Field Ion Sources. *J. Vac. Sci. Technol. 1979; 16(2); p181-183.*

Franks, J. Atom Beam Source *Vacuum* 1984; 34(1-2); p 259-261.

Fritzler, S., Malka, V., Grillon, G., Rouseau, J. P., Burgy, F., Lefebvre, E., d'Humieres, E., McKenna, P., & Ledingham, K. W. D. Proton Beams Generated with High-Intensity Lasers: Applications to Medical Isotope Production. *Applied Physics Letters. 2003; 83(15); p3030-3041.*

Geist, W. H., Brune, C. R., Karwowski, E. J. Ludwig E. J., Veal, K. D., & Hale, G. M. The ^{3}He(d,p)^{4}He Reaction at Low Energies. *Physical Review C. 1999; 60.*

Godechot, X., bernardet, H., & Lejeune. C. Optimization and Performance of a Saddle-Field Ion Source. *Rev. Sci. Instr. 1990; 61(10); p2608-2613.*

Griffiths, G. M., Larson, E. A., & Robertson, L. P. The Capture of Protons by Deuterons. *J. Canadian J. of Phys. 1962; 40(4); p 402.*

Guillaume, M., Luxen, A., Nebeling, B., Argentini, M., Clark, J. C., & Pike, V. W. Recommendations for Fluorine-18 Production.. *Appl. Radiat. Isot. 1991; 42(8); p 749-762.*

Harada, M. Watanabe, Y. Yamamoto, A. Yoshioka, S. Sato, K. Nakashima, T. Ijiri, H. Yoshida, H. Uozumi, Y. Koori, N. Meigo, S. Iwamoto, O. Fukahori, T & Chiba, S. The 12C(p,`3alpha) Breakup Reaction Induced by 14, 18 and 26 MeV Protons.. *J. of Nuclear Science and Technology. 1999; 36(4); p 313.*

Harrold, P. J., & Delchar, T. A. Discharge Characteristics of A Saddle-Field Ion Source. *J. Phys.D. Appl. Phys 1989; 22; p1275-1280.*

Hertel, N. E., Shannon, M. P., Wang, Z. L., Valenzano, M. P., Mengesha, W., & Crowe, R. J. Neutron Measurements in the Vicinity of a Self-Shielded PET Cyclotron. *Rad. Prot. Dos. 2004;108(3); pp255-261.*

Hnatowicz, V., Perina, V., Havranek, V., Vosecek, V., Novotny, J., Vacik, J., Svoreik, V., Rybka, V., & Kluge, A. Degradation of Polyimide and Polyethyleneteraphtalate Irradiated with 150 and 200 keV Ar^{+} Ions, studied by RBS and ERD Techniques. *Nucl. Instr. & Meth. Phys. Res. B. 2000;161-163; p 1099-1103.*

Horn, K. M., Doyle, B., Segal, M. N., Hamm, R. W., Adler, R. J., & Glatstein, E. The Use of Low Energy, Ion Induced Nuclear Reactions for Proton Radiotherapy Applications. *Nucl. Instr. And Meth. B* 1995; 106; p606-617.

Kapoor, V., Barry, M., McCook, M., & Torok, F. S. An Introduction to PET-CT Imaging. *RadioGraphics. 2004; 24(2); p 523-543.*

Keller, R. High-Current Ion Sources for Ion Implantation. *Nucl. Instr. & Meth. B.* 1989; 40; p518-521.

Khan, F. M. (2003) The Physics of Radiation Therapy. Williams & Wilkins. Sydney. Australia.

Kitwanga, S., Leleux, P., Lipnik, P., & Vanhorenbeeck, J. Production of $^{14,15}O$, ^{18}F, and ^{19}Ne radioactive nuclei from (*p,n*) reactions up to 30 MeV. *Phys. Rev. C. 1990; 42, p 748–752.*

Krane, K.S. (1988). Introductory Nuclear Physics. John Wiley and Sons. USA.

Kuroda, T. Development of High Current Negative Ion Source. *Fusion Engineering and Design. 1997; 36; p143-156.*

Ledingham, K. W. D., McKenna, P., McCanny, T., Shimizu, S.,Yang, J. M., Robson, L., Zweit, J., Gillies, J. M., Bailey, J., Chimon, G. N., Clarke, R. J, Neely, D., Norreys, P. A., Collier, J. L., Singhal, R. P., Wei, M. S., Mangles, S. P.D., Nilson, P., Krushelnick, K., & Zepf, M. High Power Laser Production of Short-Lived Isotope for Positron Emission Tomography. *J. Phys. D. Appl. 2004; 37; p2341-2345.*

Macleod, A.M. & Milne, G. R. Proton Nuclear Reaction Cross Sections in Carbon and the 12C(p,p`3a) Reaction Mechanism at 13 MeV. *J. of Physics, Part A (Mathematical and General); 1972; 5; p 1252.*

Matthews, J. L., Kruse, T., Williams, M. E., Owens, O. R. & Savin, W. Radiative Capture of Protons by Deuterons at Ep = 16 MeV. *J. Nucl. Phys. A; 1974; 223(2); p 221.*

Moller, W., & Besenbacher, F. A Note on the ^{3}He + D Nuclear-Reaction Cross Section. *Nucl. Instr. Meth. 1980; 168; p 111-114.*

Muggleton, A.H. F. Nuclear Target Fabrication using a Modified Fine-Beam Saddle-Field Ion Source. *Nucl. Instr. & Meth. 1991; A303; p157-161.*

Nickles, R. J., Gatley, S. J., Votaw, J. R., & Kornguth, M. L. Fluorine Radiopharmaceuticals: Production of Reactive Fluorine-18. *Appl. Radiat. Isot. 1986; 37(8); p649-661.*

Ramirez, F. M. Bulbulian, S., Collins, C. H., Collins, K. E. A Simplified Procedure for Fluorine-18 Production Using a Nuclear Reactor. *Appl. Radiat. Isot. 1992; 43(11); p1403-1406.*

Robinson, G. D., & Hamm, R. W. Fluorine-18 Production via the O18(p,n)F18 Reaction Using the AccSys PL-7 RF Proton Linac. *AccSys Technology Technical Publication Series. 1997.* Pleasanton California. USA.

Rovner, L. H. & Chen, K. Y. MeV He^{+} Bombardment of Silicon Carbide and Carbon. *Journal of Nuclear Materials, 1976; 63; p307-312.*

Ruhlman J., Oehr, P., & Biersack, H. J. (Eds). (1999). PET in Oncology. Basics and Clinical Applications.. Springer-Verlag. Berlin, Germany.

Saied, S. O., Sullivan, J. L., & Fitch, R. K. Characterization of a Saddle Field Fast Atom Beam Source. *Vacuum. 1988; 38(2); p 111-115.*

Sarangi, D., Panwar, O. S., Kumar, S., Bhattacharyya, R. Characterisation of a Saddle Field Fast Atom Beam Source and its Application to the Growth of Diamond-like Carbon Films. *Vacuum. 2000; 58; p 609-627.*

Sharma, A., Fettouhi, A., Schinner, A. & Sigmund, P. Stopping of Swift Ions in Compounds. *Nucl. Instr. & Meth. B. 2004; 218; p19-28.*

Shrinet, V., Chaturvedi, U. K., & Nigam, A. K. A Study of Blistering in Mylar due to H^+ Ion Implantation. *Nucl. Instr. & Meth. Phys. Res. B. 1986; p 46-51.*

Sigmund, P. Theory of Sputtering. I. Sputtering Yield of Amorphous and Polycrystaline Targets. *Physical Review. 1969; 184(2); p184.*

Sigmund, P. (1981). Sputtering by Particle Bombardment. (1st Ed). Springer Verlag. Berlin.

Skopik, D. M., Weller, H. R., Roberson, N. R. & Wender, S. A. 2H(p,γ)3He Reaction Using Polarized and Unpolarized Protons. *Phys. Rev. C 1979;19(3);p 601-609.*

Sprawls, P. (1995) Physical Principles of Medical Imaging. 2nd Ed. Medical Physics Publishing. Madison, Wisconsin, USA.

Stuart, R. V., & Wehner, G. K. Sputtering Yields at Very Low Bombarding Ion Energies. *J. Appl. Phys. 1962. 33; p2345-2352.*

Takacs, S., Tarkanyi, F., Hermanne, A., & Paviotti de Corcuera. Validation and Upgrading of the Recommended Cross Section Data of Charged Particle Reactions Used for Production of PET Radioisotopes. *Nucl. Inst. & Meth. B. 2003; 211; p169-189.*

Tilbury, R. S., Dahl, J. R., Mamacos, J. P., & Laughlin, J. S. Fluorine-18 Production for Medical use by Helium-3 Bombardment of Water. *Int. J. Appl. Radiat. Isot. 1970; 21; p 277-281.*

Urbassek, H. M Effect of Surface Binding Energy on Molecular Sputtering. *J. Phys. Condens. Matter. 1992; 4; p 4871.*

Wasa, K., & Hayakawa, S. (1992) Handbook of Sputter Deposition Technology: Principles, Technology and Applications. Noyes Publications, New Jersey. USA.

Yuan-Hao Liu., Rong-Jiun Sheu., Jui-Chang Chang., KuoWei Yin., $& Shiang-Huei Jiang. A study on the [^{18}F]FDG Production Efficiency of the MINItrace™ Cyclotron in Shin Kong Memorial Hospital. *Nucl. Instr. & Meth. A. 2006; 562; p1064-1067.*

Zalm, P. C. (1989) in Handbook of Ion Beam Processing Technology. Eds: Cuomo, J. J., Rossnagel, S. M., & Kaufman, H. R. Noyes Publications, New Jersey. USA.

Ziegler, J. F., Biersack, F. J. P., & Littmark, U. (2003) The Stopping and Range of Ions in Solids, Pergamon Press, New York.

Ziegler, J. F. SRIM-2003. *Nucl. Instr. & Meth B. 2004; 219-220; p1027-1036.*